Methods and Applications in Fluorescence

CrossMark

RECEIVED
27 February 2016

REVISED
6 June 2016

ACCEPTED FOR PUBLICATION
22 June 2016

PUBLISHED
2 September 2016

PAPER

Novel benzanthrone probes for membrane and protein studies

Olga Ryzhova[1,4], Kateryna Vus[1], Valeriya Trusova[1], Elena Kirilova[2], Georgiy Kirilov[2], Galyna Gorbenko[1] and Paavo Kinnunen[3]

[1] Department of Nuclear and Medical Physics, V.N. Karazin Kharkiv National University, 4 Svobody Sq., Kharkiv 61022, Ukraine
[2] Department of Chemistry and Geography, Faculty of Natural Sciences and Mathematics, Daugavpils University, Vienibas 13, LV5401 Daugavpils, Latvia
[3] Department of Neuroscience and Biomedical Engineering, School of Science and Technology, Aalto University, FI-00076, Espoo, Finland
[4] Author to whom any correspondence should be addressed: Department of Nuclear and Medical Physics, 12-191 Staroshyskivska Str., Kharkiv 61070, Ukraine

E-mail: olya_zhitniakivska@yahoo.com

Keywords: benzanthrone dyes, lipid membranes, fibrillar protein aggregates, polarity, viscosity

Abstract

The applicability of a series of novel benzanthrone dyes to monitoring the changes in physicochemical properties of lipid bilayer and to differentiating between the native and aggregated protein states has been evaluated. Based on the quantitative parameters of the dye-membrane and dye-protein binding derived from the fluorimetric titration data, the most prospective membrane probes and amyloid tracers have been selected from the group of examined compounds. Analysis of the red edge excitation shifts of the membrane- and amyloid-bound dyes provided information on the properties of benzanthrone binding sites within the lipid and protein matrixes. To understand how amyloid specificity of benzanthrones correlates with their structure, quantitative structure activity relationship (QSAR) analysis was performed involving a range of quantum chemical molecular descriptors. A statistically significant model was obtained for predicting the sensitivity of novel benzanthrone dyes to amyloid fibrils.

1. Introduction

Benzanthrone dyes, a well known class of fluorescent probes that emit in the spectral region from yellow–green to red–purple (depending on the dye structure), have found diverse applications in a variety of fields as the components of liquid-crystal systems for electro-optic displays of the 'guest-host' type [1, 2], disperse dyes for textiles [3] and polymers [4, 5], laser dyes [6], etc. Likewise, these compounds are of great interest for biomedical research and diagnostics due to their favorable spectral characteristics, such as large extinction coefficient, marked Stokes shift; negligible fluorescence in an aqueous phase, ability to intramolecular charge transfer (ICT) within chromophoric system, occurring between electron-donating groups in C-3 position and electron-accepting carbonyl group, etc [7–9]. The ability of benzanthrone fluorophores to form ICT state gives rise to significant increase of the dye dipole moment after excitation, thereby inducing the reorientation of solvent dipoles around the excited-state dipole. This property renders these dyes highly suitable for studying the membrane-related processes, especially those coupled with the changes in polarity and viscosity of lipid bilayer [10, 11]. In the early 1970s Dobretsov and Vladimirov have demonstrated that one representative of benzanthrones 3-methoxybenzanthrone (MBA) can be effectively used to monitor the membrane structural changes caused by the shifts in cholesterol (Chol) level, temperature, pH, etc [12]. Subsequently, Yang *et al* have employed this probe as DNA intercalator [13]. Later it has been shown that other benzanthrone derivatives possess marked affinity for cellular (lymphocyte) membranes, responding to the alterations in immune status of a human organism at different pathologies [14, 15].

Our previous investigations revealed that benzanthrone dyes are capable of distinguishing between the oligomeric and fibrillar aggregates of lysozyme [16, 17]. Specifically, cumulative data from the binding and red edge excitation shift studies of several novel benzanthrones allowed us to define the parameters reflecting the dye preference to either pre-fibrillar or amyloid protein aggregates [17]. Moreover, it has been shown that benzanthrone dyes are sensitive to the distinctions in fibril morphology [18]. In our recent works we also

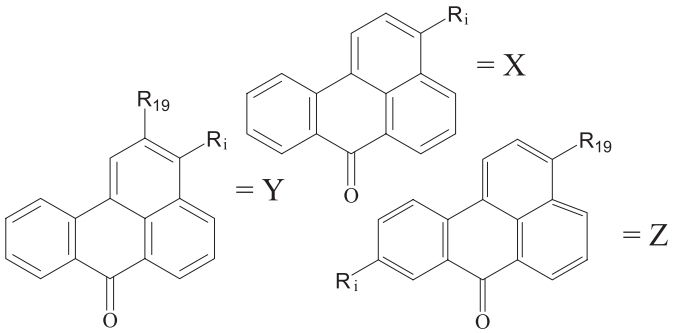

Figure 1. Structure of the examined benzanthrone dyes. The dye names and the side groups are given in table 1.

evaluated the lipid-associating ability of benzanthrones and found that their spectral responses correlate with the changes in bilayer hydration [19–21].

In the present work we extended our previous investigation of benzanthrone dyes and focused our efforts on evaluating the possibility of using newly synthesized fluorophores for probing the structural features of lipid bilayers and aggregating proteins. More specifically, our goal was several-fold: (i) to assess benzanthrone sensitivity to the changes in physicochemical characteristics of the model membranes composed of zwitterionic lipid phosphatidylcholine (PC) and its mixtures with Chol and anionic phospholipids cardiolipin (CL) and phosphatidylglycerol (PG) in different molar ratios; (ii) to assess the applicability of benzanthrones as amyloid markers; (iii) to characterize the properties of the dye binding sites within lipid or protein matrix through analyzing the red edge excitation shifts (REES); (iv) to ascertain the factors determining the lipid- and protein-associating abilities of benzanthrones.

2. Materials and methods

2.1. Materials

Chicken egg white lysozyme (HEWL) and Chol were purchased from Sigma (St. Louis, MO, USA). Bovine heart CL, 1-palmitoyl-2-oleoyl-*sn*-glycero-3-phosphocholine (PC) and 1-palmitoyl-2-oleoyl-*sn*-glycero-3-phospho-*rac*-glycerol (PG) were from Avanti Polar Lipids (Alabaster, AL). Benzanthrone dyes (figure 1 and table 1) were synthesized at the Faculty of Natural Sciences and Mathematics of Daugavpils University, Latvia as described in detail elsewhere [7, 22]. All other chemicals were of analytical grade and used without further purification.

2.2. Preparation of lipid vesicles

Lipid vesicles composed of PC and PC mixtures with CL, PG or Chol were prepared using the extrusion technique. A thin lipid film was first formed of the lipid mixtures in chloroform by removing the solvent under a stream of nitrogen. The dry lipid residues were subsequently hydrated with 20 mM HEPES, 0.1 mM EDTA, pH 7.4 at room temperature to yield lipid concentration 1 mM. Thereafter, lipid suspension was extruded through a 100 nm pore size polycarbonate filter (Millipore, Bedford, USA). In this way, 10 types of lipid vesicles containing PC and 5.3, 11.1 or 25 mol% CL, 10, 20 or 40 mol% PG and 10, 20 or 30 mol% Chol, with the content of phosphate being identical for all liposome preparations. Hereafter, liposomes containing10, 20 or 40 mol% PG are referred to as PG10, PG20 or PG40, respectively, while liposomes bearing 5.3, 11.1 or 25 mol% CL are denoted as CL5, CL11 or CL25, respectively. Accordingly, liposomes with Chol content 10, 20 or 30 mol% are marked as Chol10, Chol20 and Chol30, respectively.

2.3. Preparation of lysozyme fibrils

The reaction of lysozyme fibrillization was conducted at 60 °C by continuous shaking of lysozyme solution (20 mg ml^{-1}) in 10 mM glycine buffer (pH 1.6) during 19 d [23, 24]. The obtained aggregates, below referred to as F_{acs}, were used for the screening of the most prospective amyloid tracers of a benzanthrone series. For the investigation of the dye sensitivity to the distinctions in fibril morphology we used other two types of lysozyme fibrils: (i) aggregates (F_{ac}), grown by the protein (10 mg ml^{-1}) incubation without shaking in 10 mM glycine buffer (pH 2.2) at 60 °C during 6 d [18]; and fibrils (F_{eth}) prepared by dissolving the protein (3 mg ml^{-1}) in deionized water with subsequent slow addition of ethanol to a final concentration 80%, followed by a constant agitation of a sample at 25 °C during 30 d [18].

2.4. Steady-state fluorescence measurements

Steady-state fluorescence spectra were recorded with LS-55 (Perkin-Elmer Ltd, Beaconsfield, UK) or Varian Cary Eclipse (Varian Instruments, Walnut Creek, CA) spectrofluorimeters equipped with a magnetically stirred, thermostated cuvette holder. Fluorescence measurements were performed at 20 °C using 10 mm path-length quartz cuvettes. The excitation and emission slit widths were set at 10 nm. Excitation wavelengths and emission maxima of the examined dyes are given in table 2. Quantum yields of the examined dyes were calculated using rhodamine 101 as a standard according to the formula:

Table 1. Chemical structures of novel benzanthrone dyes.

Dye	Structure	Dye	Structure	Dye	Structure
A4	X-R1	A6	X-R2	A8	X-R3
AM1	X-R4	AM2	X-R5	AM15	X-R6
AM3	X-R7	AM4	X-R8	AM12	X-R9
ABM	X-R10	AM18	X-R11	IBH	X-R12
IAH	X-R13	FA	X-R14	ISH	X-R15
AM17	X-R16	AM20	X-R17	AM19	X-R18
AM21	X-R19	P11	X-R20	P14	X-R21
AM2-23	Y-R5	AM4-23	Y-R8	AM15-23	Y-R6
AM18	Y-R11	3AM39	Z-R7	P9	X-R23
P10	X-R24				

R1	R2	R3	R4
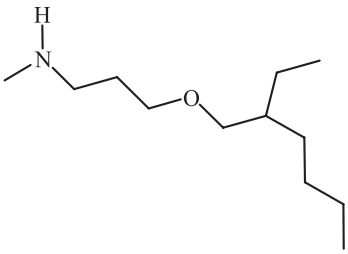	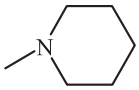	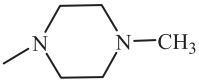	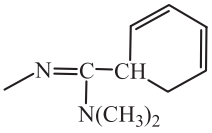
R5	**R6**	**R7**	**R8**
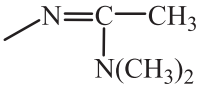	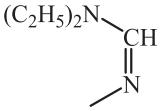	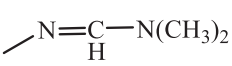	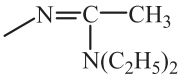
R9	**R10**	**R11**	**R12**
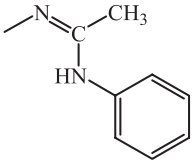	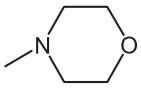	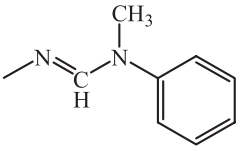	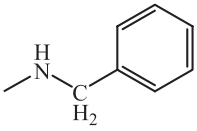
R13	**R14**	**R15**	**R16**
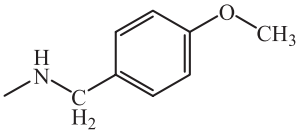	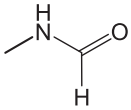	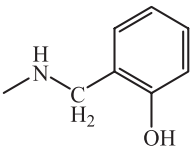	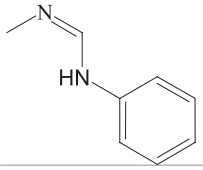
R17	**R18**	**R19**	**R20**
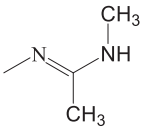	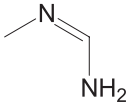	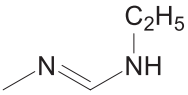	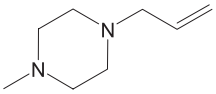
R21	**R22**	**R23**	**R24**
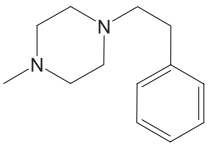		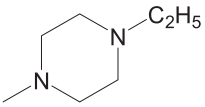	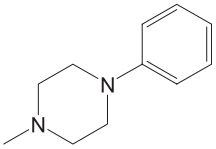

Table 2. The basic photophysical characteristics, partition coefficients and quantum yields of benzanthrone dyes in different systems.

	Ethanol				PC		CL5		CL10		Chol30	
Dye	λ_A, nm	λ_F, nm	lg ε	Q_0	Q	$K_p \times 10^4$	Q	$K_p \times 10^4$	Q	$K_p \times 10^4$	Q	$K_p \times 10^4$
AM1	470	649	4.27	0.005	0.06	2.7 ± 0.2	0.06	3.0 ± 0.3	0.05	2.8 ± 0.3	0.07	3.1 ± 0.1
AM2*	470	656	4.2	0.003	0.07	0.4 ± 0.1	0.05	0.5 ± 0.1	0.07	0.7 ± 0.05	0.06	0.5 ± 0.04
AM3*	469	636	4.07	0.013	0.44	0.8 ± 0.2	0.41	0.8 ± 0.04	0.45	0.78 ± 0.01	0.46	0.84 ± 0.07
AM4*	472	657	4.19	0.002	0.38	1.3 ± 0.2	0.42	1.4 ± 0.15	0.41	1.1 ± 0.17	0.43	0.97 ± 0.12
ABM	444	644	4.33	0.008	0.27	6.4 ± 0.7	0.32	8.2 ± 0.4	0.5	10.3 ± 0.9	0.36	6.9 ± 0.3
A6	455	654	4.01	0.018	0.44	11 ± 1.5	0.52	9.2 ± 0.9	0.6	8.4 ± 0.7	0.49	8.7 ± 0.5
A8*	444	637	3.93	0.015	0.6	0.9 ± 0.07	0.5	3.4 ± 0.05	0.48	6.2 ± 1.6	0.49	1.7 ± 0.27
A4	530	651	4.19	0.0008	0.1	1.0 ± 0.04	0.09	1.1 ± 0.1	0.09	0.9 ± 0.1	0.23	0.9 ± 0.01
AM12*	469	628	3.85	0.009	0.6	18 ± 0.8	0.5	8.7 ± 0.3	0.3	5.8 ± 0.6	0.24	15 ± 1.5
AM15*	475	632	4.15	0.005	0.6	6.1 ± 0.2	0.47	2.7 ± 0.2	0.36	1.6 ± 0.05	0.3	4.9 ± 0.4
AM18*	465	618	3.53	0.004	0.7	12 ± 0.8	0.4	9.7 ± 0.6	0.2	7.7 ± 0.5	0.5	7.8 ± 0.5
IAH*	524	644	3.6	0.002	0.06	4.8 ± 0.5	0.05	7.6 ± 0.5	0.04	5.4 ± 0.1	0.04	6.8 ± 0.8
IBH*	531	642	3.8	0.001	0.13	6.0 ± 0.4	0.06	11 ± 0.6	0.03	11 ± 0.4	0.02	9.8 ± 0.7
ISH*	529	644	2.82	0.001	0.09	6.1 ± 0.5	0.08	8.8 ± 0.4	0.07	7.0 ± 0.4	0.1	6.2 ± 0.2
3AM39	474	645	4.03	0.009	0.4	2.5 ± 0.1	0.3	5.5 ± 0.2	0.4	9.0 ± 0.4	0.6	3.4 ± 0.1
AM2-23	451	638	4.02	0.004	0.5	5.1 ± 0.2	0.4	7.6 ± 0.2	0.3	9.8 ± 0.7	0.4	8.8 ± 0.4
AM4-23	462	642	4.06	0.007	0.3	4.1 ± 0.9	0.27	10 ± 1.7	0.23	11.4 ± 0.5	0.25	4.4 ± 0.7
AM15-23	448	633	4.02	0.004	0.2	6.7 ± 1.3	0.4	8.3 ± 0.2	0.3	9.2 ± 0.9	0.5	10 ± 1.4
AM18-23	448	624	3.72	0.019	0.18	8.8 ± 1.3	0.2	9.2 ± 1.8	0.22	9.3 ± 1.7	0.3	8.9 ± 0.3
AM20	443	640	4.02	0.007	0.3	4.1 ± 0.1	0.4	9.8 ± 0.3	0.42	10.1 ± 0.5	0.5	7.1 ± 0.9
AM19	421	549	4.39	0.12	0.18	13.3 ± 0.7	0.12	14 ± 0.2	0.15	12.8 ± 1.6	0.18	13 ± 1.2
AM21	446	554	3.99	0.03	0.23	1.9 ± 0.3	0.32	7.7 ± 0.7	0.18	8.1 ± 1.2	0.22	1.5 ± 0.6
P9	446	647	4.01	0.019	0.4	2.3 ± 0.1	0.33	4.1 ± 0.2	0.3	8.1 ± 0.7	0.4	15 ± 1.2
P14	452	639	3.61	0.022	0.1	15 ± 2.6	0.3	14.7 ± 0.9	0.3	15.4 ± 2.1	0.12	14.9 ± 0.6
FA	420	554	3.54	0.05	0.08	9.1 ± 1.5	0.08	8.8 ± 0.9	0.09	9.0 ± 1.3	0.07	9.2 ± 0.7
P11	452	572	4	0.0013	Not determined							
P10	446	589	4	0.007	Not determined							
AM17	464	673	4.15	0.008	Not determined							

Note: Parameters given for dyes marked with asterisk have been reported in our previous works [*].

$$Q = \frac{Q_s(1-10^{-A_s})S_p}{(1-10^{-A_p})S_s} \cdot \frac{n_p^2}{n_s^2} \quad (1)$$

where Q_s is the standard quantum yield, S_p and S_s are the areas under the fluorescence spectra of the dye and standard, respectively, A_p and A_s are absorbances of the dye and standard at a certain excitation wavelength, n_p and n_s are refractive indexes of the measured dye solution and standard, respectively.

2.5. Time-resolved fluorescence measurements

Time-resolved fluorescence intensity decays of benzanthrone dyes were measured using a Photon Technology International spectrofluorometer equipped by GL-302 Dye Laser (Canada). This machine uses GL-3300 Nitrogen Laser that delivers a crisp pulse at 337 nm. The solution of LC 4230 (POPOP) laser dye (Kodak, USA) in a mixture of toluene with ethanol was used to excite benzanthrone dyes at 421 nm. Instrument response functions were measured at the excitation wavelength using the colloidal silica (Ludox) as a scatterer. To get smooth curves the final decay profile of each dye was obtained as the average of 6 repeats. The resulted data were fitted by biexponential function using Felix-GX software:

$$I(t) = \sum_{i=1}^{n} \alpha_i \exp(-t/\tau_i) \quad (2)$$

where τ_i and α_i are decay times and pre-exponential coefficients, n is the number of fluorescence lifetime components. The goodness of each fit was characterized by the value of reduced chi-square, weighted residuals and autocorrelation function of the weighted residuals. A fit was considered good when χ^2 fell within the range of 0.8–1.2, and the plots of weighted residuals and autocorrelation function were randomly distributed around zero [11].

The average fluorescence lifetime ($\langle\tau\rangle$) of the dyes in the presence of liposomes was calculated using the following equation [11]:

$$\langle\tau\rangle = \frac{\sum_i \alpha_i \tau_i^2}{\sum_i \alpha_i \tau_i} \quad (3)$$

2.6. Partitioning model

The binding of benzanthrone dyes to model membranes has been analyzed in terms of partition model [25]. The total concentration of the dye distributing between aqueous and lipid phases (Z_{tot}) can be represented as:

$$Z_{tot} = Z_F + Z_L \quad (4)$$

where subscripts F and L denote free and lipid-bound dye, respectively. The coefficient of dye partitioning between the two phases (K_P) is defined as:

$$K_P = \frac{Z_L V_W}{Z_F V_L} \quad (5)$$

where V_W, V_L are the volumes of the aqueous and lipid phases, respectively. Given that under the employed experimental conditions the volume of lipid phase is much less than the total volume of the system V_t, we assume that $V_W \approx V_t = 1\,\mathrm{dm}^3$. It is easy to show that

$$Z_F = \frac{Z_{tot} V_W}{V_W + K_P V_L} = \frac{Z_{tot}}{1 + K_P V_L} \quad (6)$$

The dye fluorescence intensity measured at a certain lipid concentration can be written as:

$$I = a_f Z_F + a_L Z_L = Z_F\left(a_f + a_L \frac{K_P V_L}{V_W}\right) = Z_F(a_f + a_L K_P V_L) \quad (7)$$

where a_f, a_L represent molar fluorescence of the dye free in solution and in a lipid environment, respectively. From the equations (6) and (7) one obtains:

$$I = \frac{Z_{tot} V_W (a_f + a_L K_P V_L)}{V_W + K_P V_L} \quad (8)$$

The volume of lipid phase can be determined from:

$$V_L = N_A C_L \sum v_i f_i \quad (9)$$

where C_L is the molar lipid concentration, f_i is mole fraction of the ith bilayer constituent, v_i is its molecular volume taken as 1.58 nm^3, 3 nm^3, 1.6 nm^3 and 0.74 nm^3 for PC, CL, PG and Chol, respectively [26]. The relationship between K_p and fluorescence intensity increase (ΔI) upon the dye transfer from water to lipid phase can be written as:

$$\Delta I = I_L - I_W = \frac{K_p V_L (I_{max} - I_W)}{1 + K_p V_L} \quad (10)$$

where I_L is the dye fluorescence intensity measured at a certain lipid concentration C_L, I_W is the dye fluorescence intensity in a buffer, I_{max} is the limit fluorescence in a lipid environment.

2.7. Binding model

Quantitative characteristics of the dye-lysozyme binding were determined in terms of the Langmuir adsorption model by analyzing protein-induced changes in the probe fluorescence intensity at the wavelengths, corresponding to emission maxima for each dye, as described previously [17, 18]. Briefly, approximation of the experimental dependencies of ΔI (fluorescence intensity increase) on C_P (total protein concentration), and ΔI on Z (total probe concentration), the latter being performed only for F_{acs}, by equation (11) allowed us to determine the dye-protein binding parameters—association constant (K_a), binding stoichiometry (n) and molar fluorescence (α), characterizing the difference between molar fluorescence of the bound and free dye:

$$\Delta I = 0.5\alpha\left[Z + nC_P + 1/K_a - \sqrt{(Z + nC_P + 1/K_a)^2 - 4nC_P Z}\right] \quad (11)$$

2.8. Quantum-chemical calculations

The energy of the highest occupied molecular orbital (E_{HOMO}), the energy of the lowest unoccupied molecular orbital (E_{LUMO}), the solvent-accessible area (CAr), the cosmo volume (molecular volume) (CV), the molecular length (L), height (H) and width (W), polarizability of the molecule at the electric field strength 0 eV (P), the total charge on carbon $\sum Q(C)$ and nitrogen atoms $\sum Q(N)$ was performed by the semiempirical PM6 method using MOPAC 2012 Version10.006 W-free academic license [27]. Molecular descriptors μ_g, μ_e (the dipole moment of the ground and excited states, respectively); E_g, E_e (the energy of the ground and excited states, respectively); f (oscillator strength); ΔE_e (the energy of electronic transition $S_0 \rightarrow S_1^{abs}$ from the ground state to the lowest singlet excited state, formed immediately after photon absorption); φ (dihedral angle between the donor and acceptor); q_g, q_e (the total charge on the donor of the ground and excited states, respectively) was performed with the 6-31 G(d,p) basis set, using density functional theory (DFT) and B3LYP functional [28] with Win-Gamess (version May 1, 2013 R1), offering reasonable estimates of the ground state properties [29]. Semiempirical AM1 method with added polarization (1) and diffuse (1) functions on heavy atoms, and a polarization function on hydrogen atoms was employed for the ground state geometry optimization of the benzanthrone derivatives. Virtual Computational Chemistry Laboratory (www.vcclab.org) was used for the calculation of lipophilicity of the examined compounds ($C\log P$).

3. Results and discussion

3.1. Photophysical properties of benzanthrone derivatives

The dyes under study (figure 1 and table 1) are asymmetrical amidino- and amino- benzanthrone derivatives from yellow–green to red–purple colour. Presented in table 2 are the basic photophysical characteristics of the examined benzanthrones in ethanol: absorption maximum (λ_A); extinction coefficient (ε), emission maximum (λ_F). The examined benzanthrone dyes are characterized by the broad absorption and fluorescence spectra with absorption maxima in ethanol within a range from 420 to 530 nm

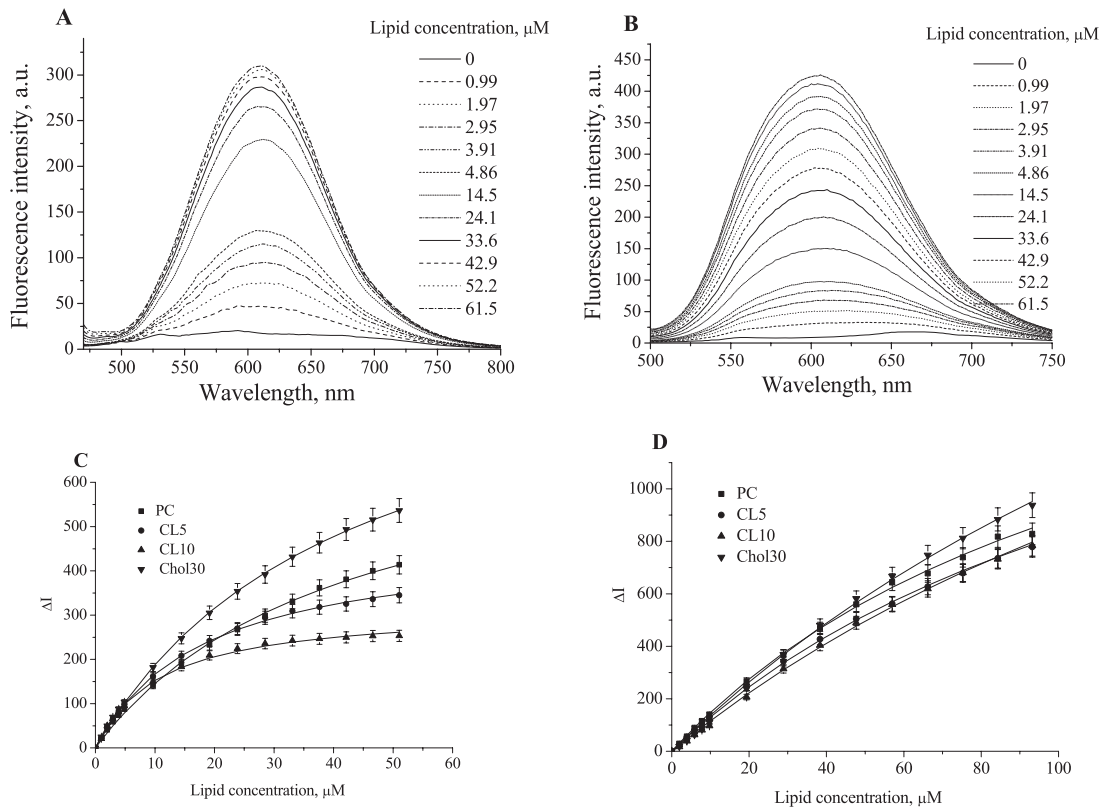

Figure 2. Typical emission spectra of benzanthrones recorded upon fluorimetric titration of AM20 (A) and 3AM39(B) with liposomes. Representative isotherms of benzanthrone binding to the model lipid membranes obtained for 3AM39 (C) and AM2 (D). Dye concentration was 1 μM.

and emission maxima from 554 to 657 nm depending on the dye structure. These dyes were found to be nearly non-emissive in buffer solution. The corresponding quantum yields of benzanthrone dyes in buffer (Q_0) are presented in table 2. As was demonstrated by Kirilova and coauthors, benzanthrone dyes displayed strong fluorescent solvatochromism due to the donor–acceptor nature of their structures [7]. Specifically, the emission maxima of the hydrophobic probes in ethanol showed ~30–70 nm shifts to the longer wavelengths as compared to those in benzene. Furthermore, a comprehensive analysis of the dye spectral properties in a range of solvents of varying polarity allowed to detect the increased Stoke's shifts and decreased quantum yields with the growth of the environmental polarity [22]. Notably, the λ_A values of ISH, IAH, IBH and A4 are red-shifted compared to other dyes, the property which is most likely associated with higher electron-donating ability of amino group compared to that of amidino group [2, 4, 22].

3.2. Association of benzanthrone dyes with model lipid membranes

At the first step of the study it was of interest to ascertain how the dye lipid-associating ability depends on the membrane physical properties being varied through introducing anionic phospholipid (CL) or sterol (Chol) into PC bilayer. For this purpose emission spectra of 25 benzanthrone dyes were recorded in buffer solution and liposomal suspensions. Typical fluorescence spectra measured at increasing lipid concentration are presented in figures 2(A) and (B). Fluorescence intensity and quantum yield were found to increase upon the dye transfer from aqueous to lipid phase as a result of reduced polarity of the dye lipid surroundings and restricted fluorophore mobility within the lipid bilayer. To derive the dye partition coefficients in different lipid systems, experimental profiles $\Delta I(C_L)$ (figure 2) were approximated by equation(10). The resulting binding curves were hyperbolic in shape for all dyes under study (figure 2(C)) except of AM2, AM3, AM4 and IAH for which linear dependencies $\Delta I(C_L)$ were observed (figure 2(D)). This means that benzanthrones AM2, AM3, AM4 and IAH possess considerably lower lipid-associating ability compared to other dyes. It is important to point out that the quantum yields of ISH, IAH, IBH in the lipid vesicles are substantially lower compared to other dyes complicating their use in membrane studies. As seen from table 2, benzanthrone derivatives AM1, AM3, AM4, A4, AM19, P14 and FA appeared to be insensitive to the changes in membrane physical properties since inclusion of Chol or CL into PC bilayer didn't affect the partition coefficients of these dyes. However, as the partition ability of a series of benzanthrones depends on lipid bilayer composition, further it was interesting to investigate the lipid binding of the most promising fluorescent probes with a broader variation of the membrane content. To this end, the model lipid membranes were formed from PC and its mixtures with 5.3, 11.1 or 25 mol% CL, 10, 20 or

40 mol% PG and 10, 20 or 30 mol of Chol. The choice of the above components of the examined lipid systems was dictated by at least three reasons [30, 31]:

(i) CL content in the inner mitochondrial membrane does not exceed 10 mol%, but it can increase considerably till 25–30 mol% in the contact zones between the inner and outer layers of the membrane;
(ii) to assess the role of headgroup chemical nature and surface charge on the lipid-associating ability of benzanthrone dyes we employed two anionic lipids CL and PG;
(iii) since Chol exerts stabilizing influence on lipid bilayer structure, it was interesting to ascertain whether this agent can modulate spectral behavior of the examined fluorophores.

The parameters of benzanthrone partitioning into lipid bilayers of different composition are presented in table 3. It turned out that inclusion of anionic lipids and Chol has an ambiguous effect on partition ability of benzanthrone dyes since addition of CL, PG and Chol to PC bilayer gives rise to the decrease of partition coefficients compared to the neat PC membrane for fluorophores of the first group (A6, AM12, AM15 and AM18), whereas benzanthrone dyes of the second group (ABM, 3AM39, AM20, AM15-23, AM4-23, AM2-23 and P9) display the opposite behavior. Since benzanthrones under study are uncharged molecules, the observed tendencies in their behavior cannot be explained by electrostatic dye-lipid interactions and most probably result from the modulating effect of anionic lipids and Chol on the structural and dynamical properties of PC bilayer. Moreover, taking into account the fundamental differences in spectral behavior of A6, AM12, AM15, AM18, on one hand, and ABM, A8, 3-AM39, AM20, AM15-23, AM4-23, AM2-23, P9, on the other hand, it seemed reasonable to scrutinize bilayer location of these two groups of fluorophores.

Therefore, at the next step of the study red edge excitation shift (REES) approach was used to determine the properties of benzanthrone binding sites. The red edge effect is known to originate from the differences in fluorophore-solvent interactions in the ground and excited states, brought about by the changes in the dye dipole moment upon excitation and the rate of solvent reorientation around the excited state fluorophore [32]. In the steady-state fluorescence measurements REES manifests itself as a shift of emission maximum towards higher wavelengths with increasing excitation wavelength. It appeared that REES does not occur for A6, AM12, AM15 and AM18. Recent studies revealed that according to their properties along the normal to bilayer plane, lipid membranes can be divided into three regions: (i) aqueous phase with fast solvent relaxation; (ii) anisotropic polar region where solvent relaxation is restricted and slow; (iii) isotropic hydrophobic part characterized by fast solvent relaxation [33, 34]. Since REES is a characteristic of hydrophilic membrane part, the fact that AM12, AM18, AM15 and A6 did not show any shift of fluorescence maximum with the change in excitation wavelength indicates that fluorophores of the first group are localized in the nonpolar region of the lipid bilayer.

In the meantime, as can be seen in figure 3, benzanthrones of the second group exhibited REES, with the magnitude of emission shift being dependent on the probe structure. The most pronounced REES was observed for AM4-23 та AM20, while the smallest one was revealed for ABM. The REES values were found to rise in the order ABM (6 nm) → 3-AM39 (11 nm) → A8 (12 nm) → AM2-23 (13 nm) → P9 (14 nm) → AM15-23 (14 nm) → AM20 (20 nm) → AM4-23 (24 nm), indicating the increase of emission shift from ABM to AM4-23. The obtained REES values allowed us to range the dyes of the second group in accordance with depth of their bilayer location. As was proposed by Chattopadhyay *et al* (so-called 'dipstick' rule), the REES magnitude varies in direct correlation with the depth of probe penetration into membrane interior—the less the REES, the deeper probe locates [32]. Accordingly, ABM is apparently localized in the interfacial region, most likely near the lipid carbonyl groups, while the other dyes prefer the binding sites which are closer to the membrane surface.

Therefore, while attempting to interpret the observed increase of partition coefficients for fluorophores of the second group, the influence of anionic lipids and Chol on physicochemical properties of the lipid-water interface should be considered. One of the possible effects of CL, PG and Chol involves the alterations in bilayer hydration. First of all it should be noted that PC, in contrast to CL, doesn't contain donor groups for hydrogen bonds (CL is capable of forming a network of intra- or intermolecular hydrogen bonds) [35]. Shibata *et al* based on FTIR data, hypothesized that the amount of membrane-bound water increases significantly in the presence of cone-shaped CL molecules (CL enhances the hydration of ester C=O groups) [36]. These findings are in good agreement with the results of molecular dynamic simulations of CL-containing lipid membranes [35]. Likewise, the ability to increase bilayer hydration was also reported for PG and Chol. In particular, several authors demonstrated that hydroxyl group of PG can form hydrogen bonds with lipid molecules as well as with water [37, 38]. Moreover, an additional argument in favor of the increase in the degree of bilayer hydration in the presence of anionic lipids, stems from the analysis of spectral responses of a number of environment-sensitive fluorophores [39, 40]. Specifically, this effect was found by the measurements of the generalized polarization of Laurdan (2-dimethylamino-6-dodecanoylnaphthalene) in micelles composed of anionic gangliosides G1, G2, G3, and model membranes, containing dipalmitoylphosphatidylcholine (DPPC) and its mixtures with CL [41, 42]. Laurdan and Prodan (2-dimethylamino-6-propionylnaphthalene) molecules possess donor and

Table 3. Parameters of benzanthrone dye partitioning into lipid systems.

Dye	Parameter	PC	CL5	CL10	CL25	PG10	PG20	PG40	Chol10	Chol20	Chol30
ABM	$K_p \times 10^4$	6.4 ± 0.7	8.2 ± 0.4	10.3 ± 0.9	11.5 ± 1.1	6.9 ± 0.9	7.4 ± 0.7	7.7 ± 1.1	7.9 ± 0.2	8.1 ± 0.4	6.9 ± 0.3
	ΔI_{max}	197 ± 3	170 ± 3	188 ± 4	290 ± 15	224 ± 6	230 ± 0.9	244 ± 4	225 ± 5	353 ± 8	412 ± 7
A6	$K_p \times 10^4$	11 ± 1.5	9.2 ± 0.9	8.4 ± 0.7	7.8 ± 0.5	8.8 ± 0.3	8.2 ± 0.3	7.1 ± 1.1	10.1 ± 1.2	9.0 ± 0.1	8.7 ± 0.5
	ΔI_{max}	280 ± 5	319 ± 3	331 ± 8	368 ± 2	313 ± 10	354 ± 31	364 ± 21	392 ± 9	419 ± 9	423 ± 10
A8	$K_p \times 10^4$	0.9 ± 0.07	3.4 ± 0.5	6.2 ± 1.6	7.8 ± 0.5	4.2 ± 0.1	5.3 ± 0.7	8.1 ± 0.9	5.5 ± 0.5	6.4 ± 0.5	6.5 ± 0.7
	ΔI_{max}	334 ± 19	401 ± 16	514 ± 18	534 ± 20	577 ± 5	680 ± 23	632 ± 15	519 ± 21	532 ± 4	498 ± 5
AM12	$K_p \times 10^4$	18 ± 0.8	8.7 ± 0.3	5.8 ± 0.6	3.1 ± 0.8	8.1 ± 0.6	7.9 ± 0.4	5.6 ± 0.5	17 ± 1.2	14.8 ± 0.8	15 ± 1.5
	ΔI_{max}	316 ± 3	287 ± 8	267 ± 16	311 ± 14	232 ± 34	208 ± 5	197 ± 15	528 ± 8	342 ± 25	480 ± 8
AM15	$K_p \times 10^4$	6.1 ± 0.2	2.7 ± 0.2	1.6 ± 0.5	1.4 ± 0.4	4.1 ± 0.5	3.4 ± 0.5	2.9 ± 0.8	6.2 ± 0.3	5.7 ± 1.4	4.9 ± 0.4
	ΔI_{max}	401 ± 12	373 ± 15	353 ± 58	323 ± 12	321 ± 21	297 ± 16	281 ± 20	385 ± 11	342 ± 48	280 ± 9
AM18	$K_p \times 10^4$	12 ± 0.8	9.7 ± 0.6	7.7 ± 0.5	5.4 ± 0.7	8.4 ± 0.7	6.9 ± 0.5	3.7 ± 0.6	9.6 ± 1.1	8.1 ± 0.7	7.8 ± 0.5
	ΔI_{max}	542 ± 10	417 ± 23	334 ± 7	401 ± 14	365 ± 13	402 ± 5	423 ± 25	487 ± 23	455 ± 31	554 ± 14
3AM39	$K_p \times 10^4$	2.5 ± 0.1	5.5 ± 0.2	9.0 ± 0.4	12.8 ± 1.2	3.6 ± 0.7	5.2 ± 0.3	7.4 ± 0.4	2.7 ± 0.3	2.9 ± 0.2	3.4 ± 0.1
	ΔI_{max}	749 ± 24	471 ± 4	315 ± 4	286 ± 9	694 ± 11	444 ± 20	370 ± 9	821 ± 13	808 ± 65	1099 ± 65
AM20	$K_p \times 10^4$	4.1 ± 0.1	9.8 ± 0.3	10.1 ± 5	12 ± 0.8	9.4 ± 0.6	12.4 ± 0.8	14.4 ± 1.3	7.1 ± 0.9	7.5 ± 0.8	8.2 ± 0.7
	ΔI_{max}	458 ± 4	334 ± 3	303 ± 4	237 ± 4	253 ± 5	190 ± 3	181 ± 4	354 ± 16	314 ± 8	382 ± 10
AM15-23	$K_p \times 10^4$	6.7 ± 1.3	8.3 ± 0.2	9.2 ± 0.9	9.4 ± 0.5	7.7 ± 1.5	8.4 ± 0.6	9.2 ± 0.5	11.1 ± 0.8	11.9 ± 0.9	10 ± 1.4
	ΔI_{max}	399 ± 28	472 ± 4	373 ± 9	563 ± 25	393 ± 11	385 ± 11	386 ± 9	716 ± 21	824 ± 14	722 ± 25
AM4-23	$K_p \times 10^4$	4.1 ± 0.9	10 ± 1.7	11.4 ± 0.5	6.3 ± 1.2	7.8 ± 0.5	8.5 ± 1.2	8.7 ± 0.8	4.1 ± 0.4	4.3 ± 0.7	4.4 ± 0.7
	ΔI_{max}	409 ± 53	259 ± 17	230 ± 16	310 ± 27	152 ± 6	171 ± 9	227 ± 9	362 ± 15	386 ± 5	424 ± 43
AM2-23	$K_p \times 10^4$	5.1 ± 0.2	7.6 ± 0.2	9.8 ± 0.7	11.4 ± 0.5	7.5 ± 1.2	8.4 ± 0.1	9.9 ± 2.1	5.4 ± 0.5	8.0 ± 1.6	8.8 ± 0.4
	ΔI_{max}	727 ± 12	653 ± 7	524 ± 1	498 ± 7	449 ± 37	410 ± 0.25	445 ± 15	514 ± 14	455 ± 43	411 ± 31
P9	$K_p \times 10^4$	2.3 ± 0.1	4.1 ± 0.2	8.1 ± 0.7	9.6 ± 0.4	4.4 ± 0.4	6.2 ± 0.7	8.4 ± 0.2	12.6 ± 1	13 ± 0.8	15 ± 1.1
	ΔI_{max}	513 ± 25	448 ± 10	467 ± 5	502 ± 9	303 ± 3	284 ± 7	286 ± 16	238 ± 6	312 ± 11	355 ± 10

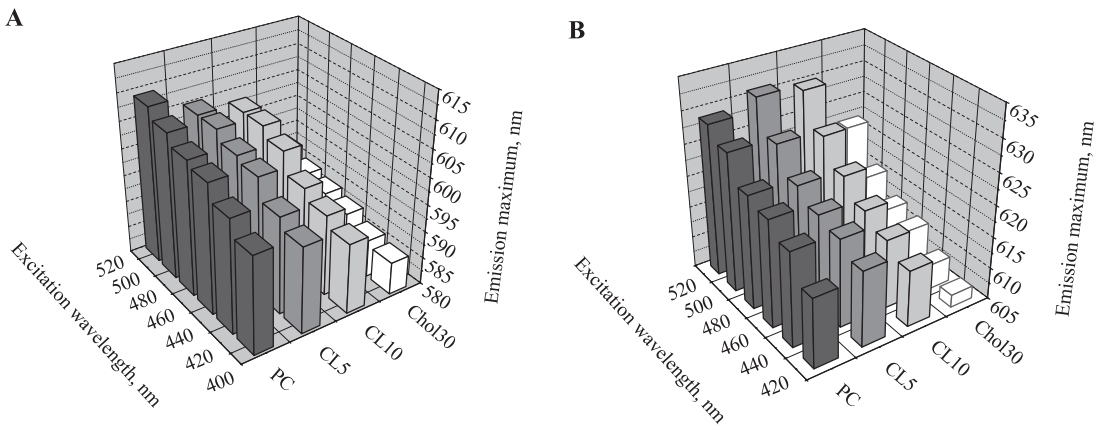

Figure 3. REES dependencies observed for 3AM39 (A) and AM2-23 (B) in different lipid systems. Dye concentration was 1 μM. Lipid concentration was 51 μM.

acceptor moieties, high ground and excited state dipole moments, which are also the characteristic features of benzanthrones [22, 43]. The two emission bands of the dyes are associated with a pair of non-relaxed (or locally excited) and solvent-relaxed (or twisted internal charge transfer) S1 states, the latter being predominant in polar solvents. Fluorescence emission maxima and lifetimes of Laurdan and Prodan are highly sensitive to the presence of water in the membrane [44, 45]. Specifically, they show long-wavelength spectral shifts ~50 nm and the shorter excited state lifetimes on the bilayer transition from the gel to the fluid phase [44, 46]. Furthermore, the novel dye 2-amino-N-hexadecyl-benzamide (Ahba) was also sensitive to the modifications of the bilayer core and headgroup region, as revealed by the steady-state and time-resolved anisotropy measurements [46]. A wealth of evidence indicates that Chol is also capable of inducing the elevation of water content in polar region of lipid bilayer [47]. Specifically it was shown that Chol inclusion into PC bilayer alters lipid packing density allowing a greater number of water molecules to penetrate in the membrane headgroup region [47]. Another support to the idea that ABM, A8, 3-AM39, AM20, AM15-23, AM4-23, AM2-23 and P9 can be employed as reporters of the changes in membrane polarity comes from 2 to 5 nm shifts of fluorescence maxima in the presence of anionic lipids and Chol compared to those observed in neat PC bilayer.

To explain the decrease of partition coefficients of A6, AM 12, AM 15 and AM18 in the presence of CL, PG and Chol, we should search for the mechanism that may underlie the effect of these lipids on physicochemical characteristics of a hydrophobic region of lipid bilayer. Specifically, liposomes composed of 1-palmitoyl-2-oleo yl-*sn*-glycero-3-phosphocholine (POPC) are in a fluid phase at 20 °C [48]. However, similar to other lipids in a fluid phase, they form liquid ordered state, possessing higher acyl chain order, when more than 20% Chol is introduced into the bilayer [49, 50]. Since in liquid-crystalline lipid phase Chol can produce tighter lateral packing of lipid molecules, the observed K_p decrease can be a consequence of Chol condensing effect on PC bilayer [26]. The situation becomes more complicated in the case of CL-containing membranes, where partition coefficient is reduced in value, since the ordering effect of CL on zwitterionic lipid bilayer is still a matter of controversy. Particularly, recent monolayer study revealed that the order of PC hydrocarbon chains increases upon CL inclusion [51]. However, fluorescence anisotropy measurements indicate that inclusion of up to 20 mol% CL in PC bilayer does not change bilayer fluidity [52]. Besides, on the basis of FTIR data Shibata *et al* [36] showed that CL negative charge tends to move the N^+ end of P–N dipole parallel to the membrane surface, thereby causing the rearrangement of water bridges at the bilayer surface and stabilizing in such a way the intermolecular hydrogen-bonded network including hydrational water. Interestingly, it was found that PG also exerts a stabilizing influence on zwitterionic bilayers [53]. The changes in hydration extent is thought to considerably affect molecular organization of a lipid bilayer, since the increase of water content in headgroup region was reported to modify the alignment of choline–phosphate dipole and lateral packing of hydrocarbon chains [54]. Presumably, the above factors prevent partitioning of A6, AM12, AM15 and AM18 in the CL- and PG-containing lipid bilayers, so we can assume that these dyes are sensitive to the changes in membrane packing density.

To better characterise the membrane partitioning of the examined compounds, in the following experiments we performed time-resolved fluorescence measurements for five fluorophores of the second group (ABM, AM4-23, AM20, 3AM39, AM2-23) and A6 which belongs to the first group of the dyes. The representative time-resolved fluorescence intensity decays of benzanthrones together with the parameters responsible for goodness of each fit are given in figure 4 and table 4. As can be seen from table 4, the fluorescence intensity decays in lipid membranes are adequately fitted by biexponential function where the longer lifetime component (τ_l) corresponds to the lifetime of the lipid-bound dye (lower environmental

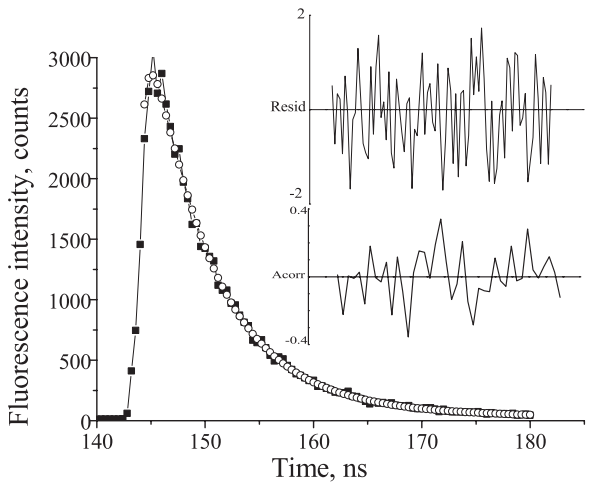

Figure 4. Time-resolved fluorescence intensity decay of ABM in PC liposomes (■), together with its exponential fit (○). Concentration of ABM was 2.4 μM. The excitation wavelength was 460 nm and emission was monitored at 600 nm. Lipid concentration was 33 μM. Shown in insets are the weighted residuals and autocorrelation function of weighted residuals.

polarity compared to buffer solution), while the shorter component accounts for the free dye in buffer (polar environment). The data presented in table 4 indicate that inclusion of anionic lipids PG, or CL and Chol into PC membrane leads to significant variations in fluorescence lifetimes of benzanthrones (τ_1 and τ_2), as well as in fractional contributions of each decay time to the overall intensity (α_1 and α_2).

Generally, while exploring the fluorescence decay profiles the parameter, such as the average fluorescence lifetime is used (equation (3)) [11]. As can be seen from table 4, inclusion of CL, PG and Chol into PC bilayer gives rise to the increase of $\langle\tau\rangle$ values compared to the neat PC membranes. To interpret this fact, one should bear in mind that the excited-state dipole moments of benzanthrone dyes are rather high compared to the ground-state counterparts, pointing to a substantial redistribution of the π-electron densities in a more polar excited state [11, 20, 22]. As a result, significant change in the dipole moment upon excitation indicates that the excited state is a twisted intramolecular charge-transfer (TICT) in nature. Many fluorescent compounds, especially those with flexible skeletons in the excited state show lifetime increase due to their sensitivity to membrane dynamics [11]. Indeed, as mentioned above, fluorescence lifetimes of e.g. Laurdan and Prodan increased when the bilayer goes from the fluid to the less hydrated gel phase [44, 46]. Since, as it was hypothesized above, A6 is localized in the hydrophobic membrane region, an increase of its $\langle\tau\rangle$ values is likely a consequence of CL, PG and Chol ability to affect the packing and ordering of lipid bilayers. Obviously, A6 belongs to the group of molecular probes sensitive to rigidity of their local environment. Lipid-associating properties of ABM, AM4-23, AM20, 3AM39 and AM-23 seem to be different compared to A6, as judged from the decrease of average fluorescence lifetime in the presence of anionic lipids and Chol. According to the results of REES measurements, these dyes are localized in the polar part of lipid bilayer, so the observed decrease of $\langle\tau\rangle$ values for ABM, AM4-23, AM20, 3AM39 and AM-23 may reflect the increase of microenvironmental polarity in CL, PG and Chol-containing membranes, as was also evidenced by Laurdan and Prodan [44, 46].

At the next step of the study fluorescence anisotropy of A6, ABM, AM4-23, AM20, 3AM39 and AM-23 was measured in the various lipid systems. Fluorescence anisotropy of a membrane-bound probe is determined by the rate of its rotational diffusion. Since diffusive motions depend on free volume of the dye microenvironment [11], anisotropy values reflect the changes in lipid packing density. As illustrated in table 5, only anisotropy of A6 appeared to be sensitive to the changes in membrane composition. The observation that anisotropy values are higher in Chol-containing membranes in comparison with pure PC liposomes confirms the above hypothesis that A6 resides in the hydrophobic membrane region experiencing condensing effect of Chol.

3.3. Benzanthrone dyes as amyloid markers

In the following, it seems of importance to illustrate that applicability of the novel benzanthrones is not limited by the membrane studies. One possible application of these dyes in the protein research field involves detection and structural analysis of particular class of protein aggregates, amyloid fibrils, associated with a number of pathologies. To exemplify, here we present the data on benzanthrone interaction with the native lysozyme and F_{acs} fibrils. To estimate the quantitative parameters of the dye-protein complexation (association constant (K_a) and binding stoichiometry (n)), the experimental dependencies of fluorescence increase on the protein concentration $\Delta I(C_P)$ (figure 5) were approximated by the Langmuir adsorption model (equation (11)). Likewise, for more accurate evaluation of the dye specificity for a certain

Table 4. Fluorescence lifetimes of benzanthrone dyes in different lipid systems.

Dye	Parameter	PC	CL5	CL10	CL25	PG10	PG20	PG40	Chol30
A6	α_1	0.85	0.82	0.81	0.79	0.77	0.79	0.69	0.83
	τ_1, ns	5.46	5.59	5.75	5.81	5.74	5.82	5.99	6.58
	α_2	0.15	0.18	0.19	0.21	0.23	0.21	0.31	0.17
	τ_2, ns	0.63	0.77	0.89	0.93	1.25	1.31	1.34	1.48
	$\langle\tau\rangle$, ns	5.36	5.45	5.57	5.61	5.46	5.56	5.56	6.35
	χ^2	1.09	1.17	1.18	1.08	1.3	1.1	1.0	1.4
ABM	α_1	0.8	0.77	0.79	0.79	0.81	0.77	0.7	0.75
	τ_1, ns	6.49	6.37	6.24	6.22	6.33	6.11	5.9	8.07
	α_2	0.2	0.23	0.21	0.21	0.23	0.23	0.3	0.25
	τ_2, ns	1.98	2.11	1.57	2.12	1.92	1.83	1.95	2.96
	$\langle\tau\rangle$, ns	6.17	5.99	5.95	5.88	5.98	5.76	5.41	7.51
	χ^2	0.9	1.0	1.11	0.96	1.04	1.2	1.24	0.93
AM4-23	α_1	0.69	0.71	0.73	0.79	0.76	0.78	0.77	0.65
	τ_1, ns	5.4	5.25	5.15	4.9	5.23	4.97	4.89	5.3
	α_2	0.31	0.29	0.27	0.21	0.24	0.22	0.23	0.35
	τ_2, ns	2.2	1.92	1.99	2.1	2.2	2.14	1.97	2.03
	$\langle\tau\rangle$, ns	4.9	4.81	4.75	4.61	4.87	4.66	4.75	4.74
	χ^2	0.89	0.98	0.93	1.01	0.95	1.11	0.95	1.14
AM20	α_1	0.88	0.91	0.79	0.81	0.76	0.82	0.68	0.75
	τ_1, ns	5.61	5.37	5.4	5.3	5.8	5.64	5.9	5.29
	α_2	0.12	0.09	0.21	0.19	0.24	0.18	0.32	0.25
	τ_2, ns	1.8	1.3	1.6	1.8	2.1	1.89	2.21	2.14
	$\langle\tau\rangle$, ns	5.45	5.27	5.12	5.04	5.42	5.38	5.34	4.91
	χ^2	1.02	0.8	0.83	0.9	1.01	0.94	0.87	1.14
3AM39	α_1	0.89	0.79	0.8	0.79	0.83	0.84	0.89	0.86
	τ_1, ns	6.13	6.27	6.22	6.21	6.04	5.95	5.57	5.35
	α_2	0.11	0.21	0.2	0.21	0.17	0.16	0.11	0.14
	τ_2, ns	1.73	1.93	1.93	2	1.33	1.4	1.1	1.71
	$\langle\tau\rangle$, ns	5.98	5.96	5.91	5.89	5.83	5.75	5.46	5.17
	χ^2	0.9	0.91	0.89	1.0	1.1	1.2	1.2	0.91
AM2-23	α_1	0.72	0.71	0.71	0.72	0.71	0.8	0.72	0.75
	τ_1, ns	7.1	6.4	6.1	6.7	6.2	6.11	5.98	5.31
	α_2	0.28	0.29	0.29	0.28	0.29	0.2	0.24	0.25
	τ_2, ns	3.5	2.7	2.6	2.7	1.9	1.1	1.6	1.7
	$\langle\tau\rangle$, ns	6.52	5.86	5.58	6.16	5.74	5.78	5.57	4.95
	χ^2	0.93	0.87	0.98	0.82	0.83	1.2	1.1	1.1

protein conformation, we employed the following additional quantities: (i) I/I_0—relative fluorescence intensity increase upon the dye binding to native or fibrillar protein; (ii) I/I_{nat}—specificity of the dyes to protein fibrillar aggregates; (iii) Q—quantum yield of the fibril-bound dye. The binding characteristics of benzanthrone dyes associated with native protein and lysozyme fibrils are presented in table 6. The titration of IAH, IBH, ISH, AM21, AM19 with native lysozyme results in saturation of the binding curves only at millimolar protein concentration indicating that association constants are very low for these dyes. Notably, for majority of the dyes elevating concentrations of native lysozyme did not produce any change in the dye emission as evidenced from relatively low quantum yields of fluorophores comparable with their quantum yields in the free state. Such a behavior may be a consequence of very low affinity of benzanthrone derivatives for protein monomers. It appeared that in the presence of lysozyme fibrillar aggregates A4, IAH and IBH showed the highest fluorescence intensity increase on going from the aqueous phase to protein matrix, while the binding preferences were the best for IAH, ABM, AM4, IBH, AM12, A4, 3AM39, AM15, AM2-23 and AM18-23. Interestingly, the K_a values for A6, A8, P11, P14, ABM, AM4-23 were 2–60 times higher for native protein in comparison with fibrillar one, whereas AM1, AM4, AM12, AM15, AM18, AM2-23, P9, IAH display the opposite behavior. In addition, fluorescence maxima of A6, AM1, AM4, AM12, AM15, AM18, AM2-23, AM21, P9, A8, P11, P14, IAH, ABM and AM4-23 in monomeric protein (λ_{em}^{nat}) were shifted to the long-wavelength region relative to their position in fibrils

Table 5. Fluorescence anisotropy of benzanthrone dyes in different lipid systems.

Liposomes	ABM	A6	AM423	AM20	3AM39	AM223
PC	0.28	0.21	0.22	0.18	0.17	0.16
CL5	0.28	0.22	0.23	0.18	0.17	0.17
CL10	0.28	0.24	0.22	0.19	0.18	0.16
CL25	0.27	0.23	0.21	0.19	0.17	0.16
PG10	0.28	0.21	0.21	0.18	0.17	0.18
PG20	0.28	0.21	0.22	0.18	0.18	0.17
PG40	0.28	0.22	0.22	0.19	0.18	0.16
Chol10	0.27	0.23	0.21	0.18	0.17	0.17
Chol 20	0.27	0.25	0.22	0.19	0.18	0.17
Chol 30	0.28	0.26	0.22	0.19	0.17	0.16

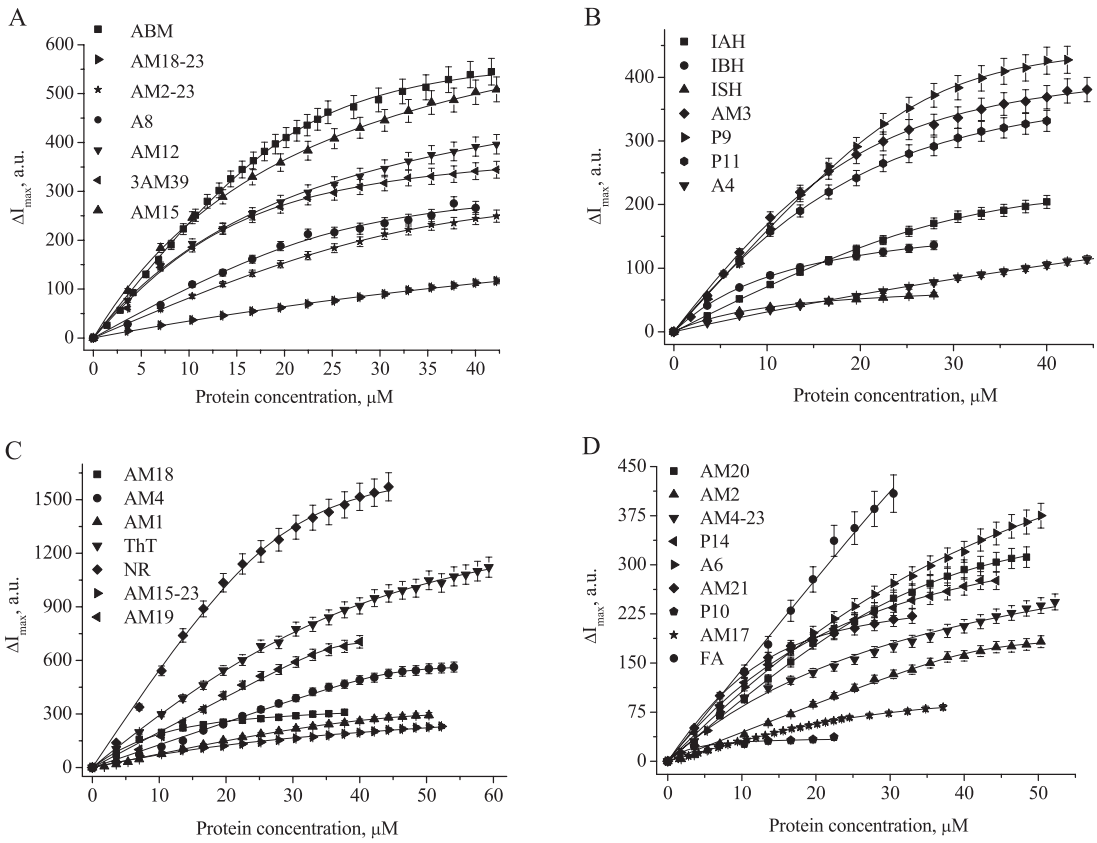

Figure 5. The isotherms of benzanthrone binding to F_{acs} fibrils. The dye concentration was 0.5 and 0.2 μM for benzanthrones and ThT, respectively.

($\lambda_{em}^{F_{acs}}$), whereas the other dyes were characterized by blue-shifted maxima (table 6). Together with fluorescence maxima position the higher K_a values observed for A6, A8, P11, P14, ABM, AM4-23 in native lysozyme are suggestive of the sensitivity of these dyes to polarity of their environment. Accordingly, the K_a values recovered for AM1, AM4, AM12, AM15, AM18, AM2-23, P9, IAH respond to the changes in viscosity of binding sites, since fluorophore surroundings is more rigid in the case of fibrillar protein [55, 56]. To compare the properties of the dyes under study with those of the classical amyloid marker, the binding parameters have been derived also for Thioflavin T (ThT). The results presented in table 6 indicate that benzanthrone dyes and ThT possess relatively high association constant 0.2–1 μM^{-1}, except of P14, AM18, AM21, AM17, AM19 and FA, for which K_a values range from 5 to 450 μM^{-1}. The values of n in the presence of amyloid fibrils were approximately equal to 0.05, although the binding stoichiometry for IAH, IBH, ISH, P10 was in the range 0.3–0.5, whereas for AM19, FA, AM4, AM17, ThT this parameter ranges from 0.01 to 0.02. Noteworthy, the classical marker ThT showed higher binding preference to amyloid fibrils in comparison with the examined dyes. However, the association constants of benzanthrones and their quantum yields were in many cases higher, giving the impetus for the use of these dyes in amyloid research. To range the examined dyes according to their specificity to fibrillar protein, three parameters have been used: fluorescence

Table 6. Binding characteristics of benzanthrone dyes associated with native lysozyme and F_{acs} fibrils.

	Native lysozyme					F_{acs}					
Dye	K_a, μM^{-1}	n	I/I_0	λ_{em}^{nat}, nm	Q_n	K_a, μM^{-1}	n	I/I_0	I/I_{nat}	λ_{em}^{Facs}, nm	Q
AM1	0.1	0.52	0	609	0.002	0.5	0.05	13	∞	617	0.15
AM2	0.33	0.23	1	655	0.004	0.2	0.12	36	16.4	616	0.16
AM3	—	—	1	653	0	0.25	0.13	14	14	610	0.18
AM4	0.36	0.027	2.2	594	0.009	0.63	0.02	44	17	624	0.33
ABM	4.9	0.54	6.4	564	0.015	0.93	0.06	75	13	603	0.35
A6	3.5	0.11	4.6	600	0.07	0.4	0.07	9	2.3	612	0.23
A8	0.17	0.09	0.8	573	0.024	0.08	0.16	8	10	598	0.47
A4	0.09	0.07	3	621	0.003	0.46	0.06	161	42	614	0.04
AM12	0.33	0.68	1.2	596	0.007	0.62	0.05	29	26	604	0.34
AM15	0.02	6	2.2	609	0.009	1	0.04	41	21	615	0.17
AM18	0.3	0.03	0	575	0.001	5.6	0.12	23	∞	597	0.08
IAH	0.002	0.057	1.6	600	0.061	0.2	0.33	135	132	602	0.2
IBH	0.001	0.1	1	616	0.042	0.33	0.43	98	81	595	0.1
ISH	0.001	0.27	1.1	626	0.034	0.96	0.4	49	37	600	0.03
3AM39	0.13	2	1.4	643	0.013	0.61	0.07	27	14	611	0.23
AM2-23	0.37	0.25	3.8	594	0.015	0.47	0.06	33	9	610	0.22
AM4-23	30	0.06	5	591	0.017	0.43	0.05	11	4	597	0.22
AM15-23	0.87	0.03	1.8	650	0.007	0.87	0.04	28	20	593	0.12
AM18-23	—	—	1	636	0	0.20	0.05	22	22	562	0.17
AM20	0.16	1.3	1.6	606	0.026	0.42	0.04	12	3.4	597	0.36
AM19	0.003	9.9	0.7	593	0.043	414	0.01	2.7	4	530	0.22
AM21	8.5	0.003	1	560	0.037	5	0.04	4	4.3	587	0.19
P9	0.13	0.7	0.9	574	0.075	0.53	0.07	13	8	599	0.34
P14	22	0.1	3	576	0.043	1.6	0.04	8	3.5	605	0.17
FA	50	0.22	1.1	655	0.098	446	0.01	2.6	1.2	531	0.19
P11	9	0.05	3.2	573	0.013	0.14	0.13	13	9	604	0.37
P10	0.024	38	0	661	0.021	0.8	0.5	3	∞	590	0.013
AM17	2.2	0.87	1.5	597	0.005	16	0.02	4	13	579	0.035
ThT	0.23	0.029	2.4	487	0.007	0.51	0.02	99	82	482	0.55

quantum yield, I/I_0 and I/I_{nat}. The amyloid specificity was found to decrease in the following row: ThT → IAH → ABM → AM4, IBH → AM12 → A4, 3AM39 → AM15, AM2-23 → AM18-23, AM3, AM18, P9, P11, ISH → AM1 → AM15-23 → AM20, A8 → AM2 → AM4-23 → P14 → A6, AM21 → P10 → AM19 → AM17 → FA.

Next, it seems of interest to discuss the nature of putative dye-fibril binding sites. The cavities, channels or grooves, abundant in the structure of amyloid fibrils, can serve as potential binding sites for benzanthrones. Several lines of evidence indicate that classical amyloid tracer ThT predominantly occupies the channels between the side chains, being the common motif in cross-β structure and running parallel to fibril axis [57, 58]. Molecular dimensions of benzanthrone dyes (~1.1–2 nm in length, ~0.7–1 nm in width and ~0.3–0.8 nm in thickness) are close to ThT size (long axis ca. 1.5 nm, short axis 0.6 nm and 0.4 nm in thickness, respectively). Thus, it cannot be excluded that fibril location of benzanthrone derivatives is similar to that of ThT. Therefore, we can suppose that benzanthrones associate with the channels formed by side chain rows consisting of 4–5 amino acid residues and running in the direction of β-sheet propagation [58, 59].

By analogy with model membranes, to confirm the above assumption concerning the fibril binding sites of benzanthrones, at the next step of the study we focused our efforts on analyzing the effect of solvent dynamics on the spectral properties of the dyes by examining the red edge excitation shift. The REES value was calculated as the difference in emission maxima of the probes excited at 450 nm and 520 nm for all dyes, excepting AM19 and FA for which the limiting excitation wavelengths were 420 and 490 nm. In the case of protein-bound dyes the presence of REES points to the restricted mobility of both the protein polar groups and the protein-bound water molecules on nanosecond scale (i.e. during the excited state lifetime) [60]. As shown in figure 6 all benzanthrones exhibited REES with emission shift in the range 0–21 nm. According to the REES values, the dyes under study can be tentatively divided into two groups: (i) the first group (P10, AM4, AM15, AM3, AM18, IAH, 3AM39, AM2-23, AM12, IBH) displaying low REES (0–7 nm) and (ii) the second

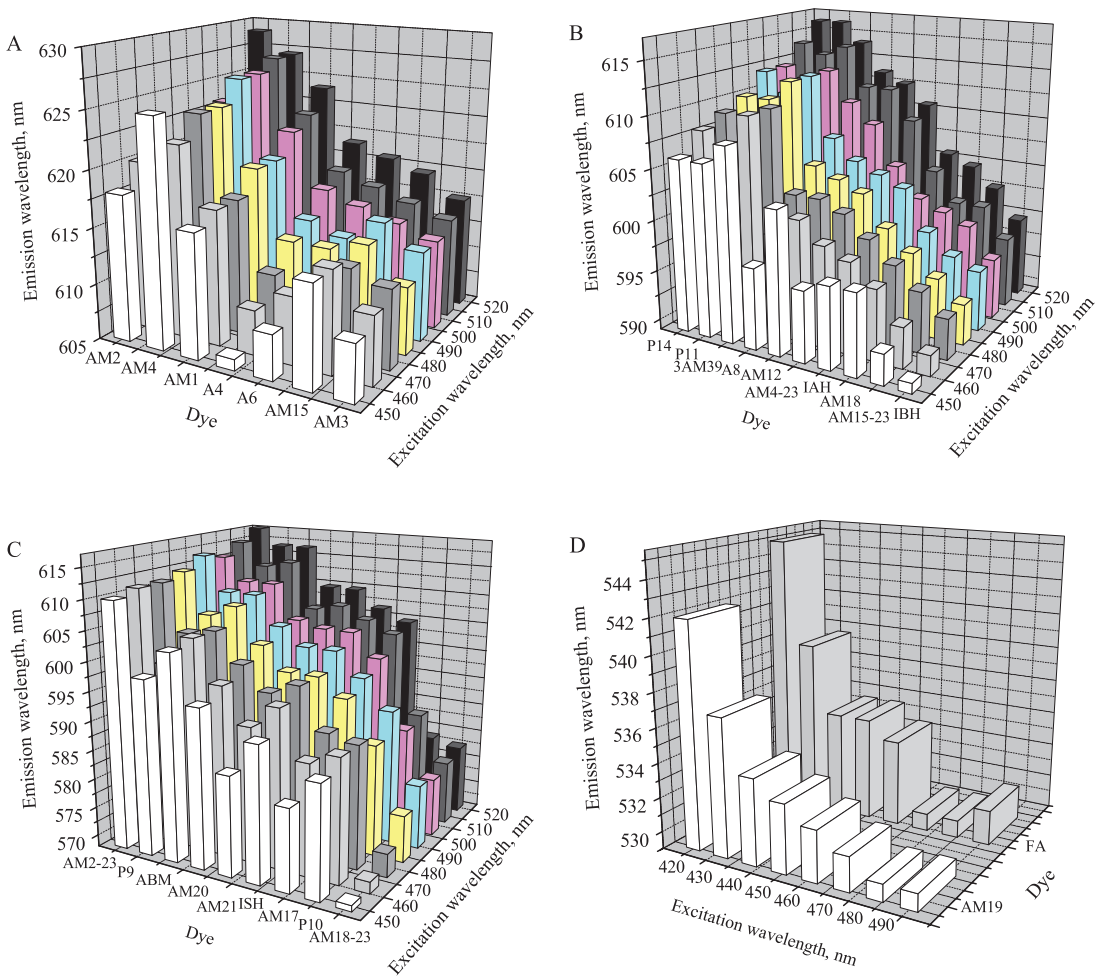

Figure 6. REES dependencies for benzanthrone dyes in the presence of F_{acs} fibrils.

group (the remaining dyes) characterized by the high REES (8–21 nm) with the average magnitude of emission shift being equal to 10 nm. The observed differences in REES values of these groups can be explained by at least two reasons: (i) heterogeneity of the binding sites, and (ii) distinct changes in the dye dipole moment after excitation. To verify the assumption that only the characteristics of binding sites affect the REES values, the dipole moment of the ground and excited states were derived from the quantum-chemical calculations (table 7). It is noteworthy at this point that all dyes belonging to the second group have more polar binding sites compared to the first group: the shifts of their emission maxima in the presence of fibrils relative to those in buffer were in the range 63–13 nm. Nevertheless, there was no correlation between the REES values and the shifts of emission maxima. Thus, one can assume that the REES values of the second group of benzanthrones are independent of microenvironmental polarity, being sensitive to the medium viscosity. On the other hand, the magnitude of REES for fluorophores of the first group whose binding sites are less polar, showed an inverse correlation with the shifts of emission maxima in fibril-bound state, suggesting that polarity essentially contribute to spectral and binding characteristics of these dyes. Taking into account that the wet 'steric zipper' interface is abundant of polar residues lined with water molecules, with every polar residue being hydrated [61], it can be supposed that benzanthrones of the second group, possessing high REES values, associate with the hydrated binding sites of amyloid fibrils. In contrast, AM4, AM15, AM3, AM18, IAH, 3AM39, AM2-23, AM12 and IBH, belonging to the first group, are most probably interact with the dry 'steric zipper' interface. At the dry 'steric zipper' interface, enriched with hydrophobic amino acids, the dye-water dipole–dipole interactions are hampered [62], thereby causing the REES weakening or even its elimination.

In our previous work 13 benzanthrone dyes were tested for their sensitivity to the variations in lysozyme fibril morphology [18]. The highest specificity to the F_{eth} amyloid aggregates was observed for AM2 and AM1, whereas A6 and A8 proved to be most specific to F_{ac} fibrils. Interestingly, A6 and A8 are representatives of benzanthrones associating with wet 'steric zipper' interface of F_{eth}, whereas AM2 presumably interacts with the dry interface, as revealed by examining the red edge excitation shift. Furthermore, all the probes were associated with the wet interface of F_{ac}. It should be noted that benzantrone dyes possess a relatively high hydrophobicity, which originates from the absence of charged groups and the presence of aromatic benzan-

Table 7. Quantum chemical characteristics of benzanthrone dyes (6-31 G (d, p), GAMESS).

Dye	μ_g, D	μ_e, D	E_g, Hartree	f	ΔE_e, cm^{-1}	E_e, Hartree	φ, degrees	q_g^{benz}	q_e^{benz}
A6	5.36	10.94	−979.2	0.21	22 592	−979	24.5	0.14	0.20
AM1	6.44	10.24	−1188	0.264	22 487	−1189	94.3	0.1	−0.022
AM2	8.03	12.06	−995.2	0.352	22 665	−995	44	0.12	0.003
AM3	6.42	9.77	−956	0.289	22 891	−956	−132.3	0.13	0.022
AM4	8.2	12.33	−1074	0.369	22 479	−1074	−43.9	0.12	−0.01
AM12	6.99	11.03	−1147.6	0.388	23 116	−1147	−45	0.16	0.059
AM15	6.76	10.23	−1035	0.292	22 979	−1034	−126.1	0.12	0.012
AM18	5.79	9.55	−1147.6	0.343	22 745	−1147	130	0.16	0.066
AM2-23	5.67	9.3	−3568	0.233	22 955	−3568	106.1	0.062	−0.034
AM21	8.27	12.03	−956	0.358	23 012	−956	33	0.15	0.057
P9	5.26	11.54	−1074	0.215	22 084	−1074	23.4	0.14	0.18
AM18-23	4.95	9.18	−3721	0.298	22 729	−3721	124.5	0.1	−0.025
A8	5.12	11.41	−1034.5	0.21	22 028	−1034	25.1	0.14	0.19
P10	4.31	20.62	−1226	0.141	20 156	−1226	26.9	0.23	0.21
P11	4.94	17.51	−1112	0.153	20 156	−1112	27.3	0.18	0.23
P14	5.67	10.94	−1305	0.249	22 269	−1305	15.4	0.19	0.24
A4	4.97	8.23	−1291.3	0.214	22 592	−1291	−124	0.14	0.037
IAH	5.96	10.08	−1169	0.254	23 124	−1169	−111.7	0.17	0.050
IBH	5.54	9.40	−1054	0.244	23 149	−1054	−113.6	0.16	0.046
ISH	6.27	10.25	−1129	0.236	23 366	−1129	−107.9	0.15	0.028
AM19	5.43	8.09	−877.4	0.213	23 100	−877	−118	0.31	0.22
FA	3.53	5.12	−897.3	0.173	24 149	−897	−130	0.44	0.38
ABM	3.83	9.82	−1015	0.204	22 165	−1015	24	0.19	0.25
AM17	3.84	26.1	−1109	0.009	21 931	−1109	−113.6	0.16	−0.63
3AM39	5.15	14.66	−3529.1	0.254	21 326	−3539	20.5	0.22	−0.05
AM4-23	5.67	9.56	−3647	0.249	22 624	−3647	−115.2	0.064	−0.05
AM20	6.76	9.84	−956	0.248	22 866	−956	−118	0.11	−0.08
AM15-23	5.57	9.47	−3608	0.259	22 955	−3608	−121.9	0.082	−0.02

throne moiety. These facts indicate that fibrils prepared by shaking most probably possess a denser packing of stacking β-sheets, creating prerequisites for fluorophore binding to dry 'steric zipper' interface. In any case, the binding parameters presented in this work confirmed our assumption about benzanthrone sensitivity to amyloid morphology.

Recently, an attempt has been made to understand how the partition ability of benzanthrone dyes depends on their physicochemical properties through analyzing a series of molecular descriptors [20]. The quantitative structure property relationship (QSPR) analysis showed high correlation between experimentally determined partition coefficients and geometrical parameters of the examined dyes, their lipophilicity and dipole moment, pointing to multiplicity of factors contributing to lipid bilayer affinity of these compounds. Therefore, it seemed of interest to develop a QSAR model for predicting the sensitivity of novel benzanthrone dyes to amyloid fibrils. For this purpose, 21 quantum-chemical descriptors for 28 tested dyes were calculated using semiempirical PM6, *ab initio* 6-31 G(d,p) methods. The obtained parameters are presented in tables 7 and 8. As seen in table 7, the changes of the dipole moments of benzanthrones after excitation fall in the range 3.3–6.3 D. The highest increases of the dipole moment were observed for P10, P11, AM17 and 3AM39 (ca ~9.5–22.3 D), while the smallest ones were found for AM19 and FA (2.7 and 1.6 D, respectively). Interestingly, this quantity showed marked positive correlation with the dye sensitivity to amyloid fibrils (see the amyloid specificity row). Indeed, the dipole moment changes determine the sensitivity of the dyes to the polarity of their local environment, thereby affecting their specificity to amyloid fibrils [63]. Comparison of the REES values with the differences $\mu_e - \mu_g$ for each dye suggests that REES is influenced by the characteristics of benzanthrone binding sites, since the dyes with significant change in the dipole moment upon excitation (A6, P9, A8, P11, P14, ABM, AM17, $\mu_e - \mu_g \sim 5.3$–22.3 D) and the dyes with small $\mu_e - \mu_g$ values (AM1, AM2, AM21, AM18-23, A4, ISH, AM19, FA, AM4-23, AM20, AM15-23, $\mu_e - \mu_g \sim 1.6$–4.2 D) exhibit substantial REES. Notably, for amidino benzanthrones (IAH, IBH, ISH, FA) the changes in the dipole moment upon excitation are smaller than $\mu_e - \mu_g$ for amino benzanthrones. Interestingly, the values of the dihedral angle between benzanthrone moiety and its substitution in C-3 position were found to fall in the range (−132°–130°), with the magnitude of φ change being more pronounced for amidino-benzanthrones, pointing to higher conjugation degree between the donor–acceptor system for amino-benzanthrone dyes [64].

Table 8. Quantum chemical characteristics of benzanthrone dyes (PM6, MOPAC).

Dye	CAr, Å^2	CV, Å^3	E_{HOMO} eB	E_{HOMO} eB	L, Å	$\sum Q(N)$	$\sum Q(C)$	$CLogP$	W, Å	H, Å	P, Å^3
A6	319	368	−8.0	−1.1	12.9	−0.30	−1.99	6.27	7.1	3.5	43.4
AM1	387	460	−8.5	−1.3	13.4	−0.72	−2.16	6.23	8.3	7.2	50.7
AM2	335	380	−8.3	−1.1	13.9	−0.78	−1.61	3.95	7.2	4.6	44.0
AM3	323	358	−8.3	−1.2	13.8	−0.7	−1.30	3.96	7.5	3.6	42.5
AM4	362	416	−8.1	−1.1	14.8	−0.51	−1.61	4.68	7.6	4.0	46.7
AM12	373	426	−8.3	−1.2	15.3	−0.49	−1.68	5.32	7.8	3.8	44.0
AM15	355	403	−8.1	−1.1	13.2	−0.84	−1.72	4.70	9.2	3.7	47.4
AM18	374	427	−8.3	−1.3	15.9	−0.47	−1.59	5.52	7.1	3.4	49.3
AM2-23	347	407	−8.4	−1.4	13.9	−0.74	−1.45	4.80	7.4	4.7	47.1
AM21	324	357	−8.5	−1.2	13.9	−0.95	−1.25	4.15	7.2	2.8	41.2
P9	358	411	−8.5	−1.3	15.8	−0.67	−2.00	4.98	7.4	3.8	45.5
AM18-23	395	454	−8.6	−1.5	16.1	−0.70	−1.41	5.27	7.8	3.8	54.9
A8	340	390	−8.5	−1.3	14.5	−0.63	−1.80	4.49	6.8	3.8	43.6
P10	389	455	−8.4	−1.4	16.7	−0.63	−2.26	6.62	7.6	4.7	52.3
P11	365	425	−8.5	−1.3	14.5	−0.62	−2.20	5.33	8.2	4.8	46.6
P14	430	507	−8.8	−1.4	18.2	−0.68	−2.62	6.47	7.4	4.3	54.8
A4	451	550	−8.4	−1.3	18.7	−0.43	−3.84	7.94	8.7	3.8	54.6
IAH	373	431	−8.5	−1.3	12.1	−0.42	−1.75	5.85	11.4	4.2	47.9
IBH	343	399	−8.5	−1.3	11.3	−0.42	−1.80	5.76	8.3	2.8	44.6
ISH	359	407	−8.3	−1.2	15.7	−0.42	−1.5	5.28	7.2	2.5	46.8
AM19	279	312	−8.6	−1.3	11.4	−0.98	−0.63	3.38	6.9	2.6	36.2
FA	278	308	−9.0	−1.7	11.7	−0.37	−0.51	3.87	6.9	2.2	35.8
ABM	312	359	−8.2	−1.3	11.8	−0.29	−1.36	4.52	7.9	3.4	41.9
AM17	363	411	−8.6	−1.5	13.9	−0.92	−1.55	6.07	7.6	6.3	46.3
3AM39	347	387	−8.4	−1.5	13.9	−0.68	−1.14	4.65	8.1	1.9	47.0
AM4-23	371	445	−8.4	−1.3	13.9	−0.85	−1.93	5.61	7.2	4.7	50.9
AM20	318	357	−8.4	−1.2	13.4	−0.79	−1.32	3.77	6.8	4.4	40.9
AM15-23	365	526	−8.4	−1.4	13.4	−0.75	−1.62	5.33	7.4	5.2	49.7

To correlate the amyloid sensitivity of benzanthrone dyes I/I_0 with a series of calculated molecular descriptors, the partial least squares regression (PLSR) was performed using the resources of www.vcclab.org/lab/pls/ [65]. Allowing for the foresaid differences between amyloid specificity of benzanthrone derivatives, it was reasonable to perform separate correlation analysis for the dyes highly sensitive to protein aggregates (with $I/I_0 \geqslant 20$ (AM18-23, 3AM39, AM15-23, AM12, AM2-23, AM2, AM15, AM4, ISH, ABM, IBH, IAH, A4) and those possessing law amyloid specificity with $I/I_0 < 20$ (FA, AM19, P10, AM17, AM21, P14, A8, AM4-23, AM20, P11, AM1, AM3, P9, A6, AM18). To determine the parameters appropriate for PLRS analysis, initially for each group of benzanthrones we performed linear correlation analysis and selected the descriptors, for which correlation coefficients with I/I_0 were higher than 0.6, while the mutual correlation coefficients between the descriptors were below 0.9 [66]. It appeared that for the first group of the probes the highest linear correlation was observed between I/I_0 and $\sum Q(N)$, $\sum Q(C)$, $CLogP$, W (correlation coefficients are 0.62, −0.74, 0.77, 0.64, respectively); whereas for the second group—with E_{HOMO}, E_{LUMO}, q_g^{benz} (correlation coefficients are 0.64, 0.60, −0.61, respectively). As seen in figure 7(A), the partial least square analysis for the benzanthrones with high sensitivity to amyloid fibrils yields a statistically significant model (Fisher's coefficients $FtY = 42.19$) with high correlation coefficient ($RY = 0.946$) and low mean absolute error ($MYE = 10.646$). In addition, the presented model has very high predictive ability (i.e. cross-validation correlation coefficient $Q^2 = 0.804$), and satisfactory values of mean squared error of cross-validation ($MSE_{cv} = 0.196$) and standard deviation of cross-validation ($RMS_{cv} = 0.446$). The opposite situation was observed for fluorophores with $I/I_0 < 20$, since a weak correlation was found. Moreover, predictive ability was relatively low ($Q^2 = 0.446$), but the RMS_{cv} and MSE_{cv} values were higher (figure 7(B)). Interestingly, the regression equation obtained for benzanthrone dyes possessing high amyloid specificity ($I/I_0 \geqslant 20$) is more stable and predictable than the early regression model of sensitivity of ThT derivatives to Aβ1-40 and insulin fibrils [65, 66].

In the following, let's dwell on the regression model derived for amyloid-specific benzanthrones in more detail (figure 7(A)). General regression equation I/I_0 contains molecular descriptors with a weak mutual correlation. The impact of each descriptor I_j on the general

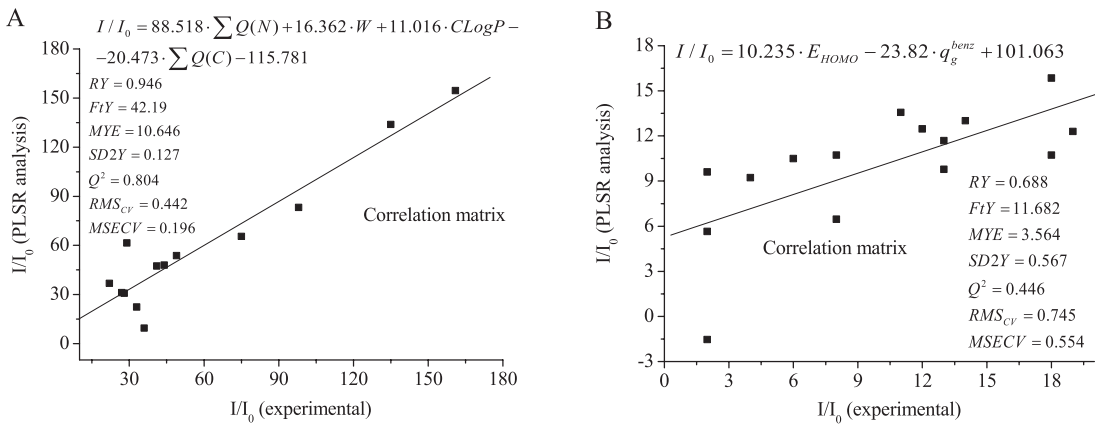

Figure 7. Linear regression curve showing relation between the theoretically calculated values of amyloid specificity and experimentally determined I/I_0 values for two groups of benzanthrone dyes: AM18-23, 3AM39, AM15-23, AM12, AM2-23, AM2, AM15, AM4, ISH, ABM, IBH, IAH, A4 ($I/I_0 \geqslant 20$) (A); and FA, AM19, P10, AM17, AM21, P14, A8, AM4-23, AM20, P11, AM1, AM3, P9, A6, AM18 ($I/I_0 \geqslant 20$) (B).

value of I/I_0 was about 0.35, −0.4, 0.32, 0.49 for $\sum Q(N)$, $\sum Q(C)$, $CLogP$, W, respectively. Based on the analysis of contribution of each independent descriptor, we can conclude that: (i) the increase in molecular width of benzanthrone dyes W exerts a positive impact on the probe amyloid specificity to F_{acs} fibrils; (ii) the marked positive effect on I/I_0 value is inherent to lipophilicity $CLogP$; (iii) the dye sensitivity to amyloid fibrils is proportional to the charge of donor group of benzanthrone molecule ($\sum Q(N)$) and decreases with lowering the total charge on benzanthrone skeleton ($\sum Q(C)$).

A marked positive correlation between amyloid specificity and W value is indicative of significant role of steric interactions in the benzanthrone complexation with fibrils and their sensitivity to the viscosity of the environment. Indeed, it was previously demonstrated that steric interactions affect the quantum yield of ThT and its derivatives associating with amyloid fibrils [66, 67]. The increase of I/I_0 value with molecular width also point to significance of aromatic interactions in benzanthrone association with lysozyme aggregates. At the same time, the observed positive correlation between amyloid specificity and lipophilicity testifies that benzanthrone binding to amyloid fibrils is controlled also by hydrophobic interactions. It is noteworthy that aromatic and hydrophobic residues significantly contribute to the ThT affinity for amyloid fibrils. Specifically, based on the results of molecular docking, Biancalana and coworkers demonstrated that ThT binds presumably to the fibril grooves formed by tyrosine and leucine [57]. An important role of aromatic interactions in ThT-fibril complexation was also reported by Wolfe *et al* [68].

Taken together, the results of QSAR analysis showed that hydrophobic ($\sim CLogP$) and van-der-Waals/ion-dipole dye protein interactions (electron-donating power of the substituent at the C-3 position ($\sum Q(N) - \sum Q(C)$) are more essential than aromatic and steric interactions (W). The obtained model could be effectively employed for preliminary selection of benzanthrone dyes with high amyloid specificity.

4. Conclusion

To summarize, the present study has been undertaken to evaluate the applicability of the novel benzanthrone dyes to monitoring the changes in physicochemical properties of lipid membranes, as well as to detection and characterization of the protein fibrillar aggregates. All the examined dyes were found to associate with liposomes and amyloid fibrils with the magnitude of binding being dependent on the dye structure. Based on comprehensive analysis of the spectral characteristics of benzanthrones bound to liposomes, we can recommend ABM, 3AM39, AM20, AM15-23, AM4-23, AM2-23 and P9 for examining membrane-related processes coupled with polarity changes. The most prospective amyloid tracers were selected from 28 studied compounds. The results of quantum-chemical calculations and QSAR analysis revealed a positive correlation between amyloid specificity of benzanthrone dyes and a series of descriptors, such as lipophilicity, molecular width of the probe and electron-donating power of the substituent at the C-3 position. A statistically significant model was obtained for predicting the sensitivity of novel benzanthrone dyes to amyloid fibrils.

References

[1] Grabchev I and Moneva I 1998 Synthesis and properties of benzanthrone derivative as luminophore dyes for liquid crystals *Dyes Pigm.* **37** 155–65
[2] Grabchev I, Moneva I, Wolarz E and Bauman D 2003 Fluorescent 3-oxy benzanthrone dyes in liquid crystalline media *Dyes Pigm.* **58** 1–6
[3] Krasovitskii B M and Bolotin B M 1988 *Organic Luminescent Materials* (New York: Wiley-VCH)
[4] Konstantinova T, Spirieva Ant and Konstantinov Hr 1998 On the photostability of some benzanthorne dye derivatives and their copolymers with methylmethacrylate *Polym. Degrad. Stab.* **60** 511–13
[5] Carlini F, Paffoni C and Boffa G 1982 New daylight fluorescent pigments *Dyes Pigm.* **3** 59–69
[6] Khrolova O R, Kunavin N I, Komlev I V, Tavrizova M A, Trofimova S I, Madii V A and Petukhov V A 1984 Spectral and

luminescence properties of phosphorylmethyl derivatives of 3-aminobenzanthrone *J. Appl. Spectrosc.* **41** 53–7
[7] Kirilova E, Kalnina I, Kirilov G and Meirovics I 2008 Spectroscopic study of benzanthrone 3-N-derivatives as new hydrophobic fluorescent probes for biomolecules *J. Fluoresc.* **18** 645–8
[8] Refat M, Aqeel S and Grabtchev I 2004 Spectroscopic and physicochemical studies of charge-transfer complexes of some benzanthrone derivatives 'luminophore dyes' with iodine as σ-acceptor *Can. J. Anal. Sci. Spectrosc.* **49** 258–65
[9] Grabchev I, Bojinov V and Moneva I 1998 Functional properties of azomethine substituted benzanthrone dyes for use in nematic liquid crystals *J. Mol. Struct.* **471** 19–25
[10] Value B 2001 *Molecular Fluorescence: Principles and Applications* (Weinheim: Wiley-VCH)
[11] Lakowicz J R 1999 *Principles of Fluorescent Spectroscopy* 2nd edn (New York: Kluwer)
[12] Dobretsov G, Dmitriev V, Pirogova L, Petrov V and Vladimirov Yu 1978 4-Dimethylaminochalcone and 3-methoxybenzanthrone as fluorescent probes to study biomembranes. III Relationship between state of hydration shell of membrane and state of phospholipids *Stud. Biophys.* **71** 189–96
[13] Yang X, Liu W-H, Jin W-J, Shen G-L and Yu R-Q 1999 DNA binding studies of a solvatochromic fluorescence probe 3-methoxybenzanthrone *Spectrochim. Acta* A **55** 2719–27
[14] Kirilova E and Kalnina I 2010 3-isopropyloxy-6-morpholino-2-phenylphenalen-1-one as lipophilic fluorescent probe for lymphocyte investigations *Appl. Biochem. Biotechnol.* **160** 1744–51
[15] Kalnina I, Klimkane L, Kirilova E, Toma M, Kizane G and Meirovics I 2007 Fluorescent probe ABM for screening gastrointestinal patient's immune state *J. Fluoresc.* **17** 619–25
[16] Gorbenko G, Trusova V, Kirilova E, Kirilov G, Kalnina I, Vasilev A, Kaloyanova S and Deligeorgiev T 2010 New fluorescent probes for detection and characterization of amyloid fibrils *Chem. Phys. Lett.* **495** 275–9
[17] Vus K, Trusova V, Gorbenko G, Kirilova E, Kirilov G, Kalnina I and Kinnunen P 2012 Novel aminobenzanthrone dyes for amyloid fibril detection *Chem. Phys. Lett.* **532** 110–15
[18] Vus K, Trusova V, Gorbenko G, Sood R, Kirilova E, Kirilov G, Kalnina I and Kinnunen P 2014 Fluorescence investigation of interactions between novel benzanthrone dyes and lysozyme amyloid fibrils *J. Fluoresc.* **24** 193–202
[19] Trusova V, Kirilova E, Kalina I, Kirilov G, Zhytniakivska O, Fedorov P and Gorbenko G 2012 Novel benzanthrone aminoderivatives for membrane studies *J. Fluoresc.* **22** 953–9
[20] Zhytniakivska O, Trusova V, Gorbenko G, Kirilova E, Kalnina I, Kirilov G and Kinnunen P 2014 Newly synthesized benzanthrone derivatives as prospective fluorescent membrane probes *J. Luminesc.* **146** 307–13
[21] Zhytniakivska O, Trusova V, Gorbenko G, Kirilova E, Kalnina I, Kirilov G, Molotkovsky J, Tulkki J and Kinnunen P 2014 Location of novel benzanthrone dyes in model membranes as revealed by resonance energy transfer *J. Fluoresc.* **24** 899–907
[22] Gonta S, Utinans M, Kirilov G, Belyakov S, Ivanova I, Fleisher M, Savenkov V and Kirilova E 2013 Fluorescent substituted amidines of benzanthrone: synthesis, spectroscopy and quantum chemical calculations *Spectrochim. Acta* A **101** 325–34
[23] Sasahara K, Yagi H, Naiki H and Goto Y 2007 Heat-induced conversion of β2-microglobulin and hen egg-white lysozyme into amyloid fibrils *J. Mol. Biol.* **372** 981–91
[24] Arnaudov L N and de Vries R 2005 Thermally induced fibrillar aggregation of hen egg white lysozyme *Biophys. J.* **88** 515–26
[25] Santos N, Prieto M and Castanho M 2003 Quantifying molecular partition into model systems of biomembranes: an emphasis on optical spectroscopic methods *Biochim. Biophys. Acta* **1612** 123–35
[26] Ivkov V and Berestovsky G 1981 *Dynamic Structure of Lipid Bilayer* (Moscow: Nauka)
[27] Schmidt M W *et al* 1993 General atomic and molecular electronic structure system *J. Comput. Chem.* **14** 1347–63
[28] Binkley J S, Pople J A and Henre W J 1980 Self-consistent molecular orbital methods. 21. Small split-valence basis sets for first-row elements *J. Am. Chem. Soc.* **102** 939–47
[29] Scheiner S 2000 Theoretical studies of excited state proton transfer in small model systems *J. Phys. Chem.* A **104** 5898–909
[30] Ohvo-Rekila H, Ramstedt B, Leppimaki P and Peter Slotte J 1990 Cholesterol interactions with phospholipids in membranes *Prog. Lipid Res.* **265** 18797–802
[31] Ardail D, Privat J, Egretcharlier M, Levrat C, Lerme F and Louitson P 1990 Mitochondrial contact sites—lipid composition and dynamics *J. Biol. Chem.* **265** 18797–802
[32] Chattopadhyay A and Mukherjee S 1999 Red edge excitation shift of a deeply embedded membrane probe: implications in water penetration in the bilayer *J. Phys. Chem.* B **103** 8180–5
[33] Raghuraman H, Kelkar D and Chattopadhyay A 2005 *Novel Insights into Protein Structure and Dynamics Utilizing the Red Edge Excitation Shift Approach in Reviews in Fluorescence* (New York: Springer)
[34] Marrink S J, Sok R M and Berendsen H J C 1996 Free volume properties of a simulated lipid membrane *J. Chem. Phys.* **104** 9090–9
[35] Dahlberg M and Maliniak F 2008 Molecular dynamics simulation of cardiolipin bilayers *J. Phys. Chem.* B **112** 11655–63
[36] Shibata A, Ikawa K, Shimooka T and Terada H 1994 Significant stabilization of the phosphatidylcholine bilayer structure by incorporation of small amounts of cardiolipin *Biochim. Biophys. Acta* **1192** 71–8
[37] Zhang Y P, Lewis R N A H and McElhaney R N 1997 Calorimetric and spectroscopic studies of the thermotropic phase behavior of the n-saturated 1,2-diacylphosphatidylglycerols *Biophys. J.* **72** 779–93
[38] Rand R P and Parsegian V A 1989 Hydration forces between phospholipid bilayers *Biochim. Biophys. Acta* **988** 351–76
[39] Klymchenko A S, Duportail G, Demchenko A P and Mely Y 2004 Bimodal distribution and fluorescence response of environment-sensitive probes in lipid bilayers *Biophys. J.* **86** 2929–41
[40] Klymchenko A S, Mely Y, Demchenko A P and Duportail G 2004 Simultaneous probing of hydration and polarity of lipid bilayers with 3-hydroxyflavone fluorescent dyes *Biochim. Biophys. Acta* **1665** 6–19
[41] Bagatolli L A, Gratton E and Fidelio G D 1998 Water dynamics in glycosphingolipid aggregates studied by LAURDAN fluorescence *Biophys. J.* **75** 331–41
[42] Suga K, Hamasaki A, Chinzaka J and Umakoshi H 2016 Liposomes modified with cardiolipin can act as a platform to regulate the potential flux of NADP + dependent isocitrate dehydrogenase *Metab. Eng. Commun.* **3** 8–14
[43] Titova T Y, Artyukhov V Y, Zharkova O M and Morozova J P 2014 Spectral-luminescent properties of laurdan molecule *Spectrochim. Acta* A **124** 64–9
[44] Vequi-Suplicy C C, Coutinho K and Lamy M T 2015 New insights on the fluorescent emission spectra of prodan and laurdan *J. Fluoresc.* **25** 621–9
[45] Khalifat N, Fournier J B, Angelova M I and Puff N 2011 Lipid packing variations induced by pH in cardiolipin-containing bilayers: the driving force for the cristae-like shape instability *Biochim. Biophys. Acta* **1808** 2724–33
[46] Vequi-Suplicy C C, Lamy M T and Marquezin C A 2013 The new fluorescent membrane probe Ahba: a comparative study with the largely used laurdan *J. Fluoresc.* **23** 479–86
[47] Pasenkiewicz-Gierula M, Rog T, Kitamura K and kusumi A 2000 Cholesterol effects on the phosphatidylcholine bilayer polar region: a molecular simulation study *Biophys. J.* **78** 1376–89
[48] Kučerka N, Nieh M-P and Katsaras J 2011 Fluid phase lipid areas and bilayer thicknesses of commonly used phosphatidylcholines as a function of temperature *Biochim. Biophys. Acta* **1808** 2761–71
[49] Favela-Rosales F, Carbajal-Tinoco M D and Ortega-Blake I 2014 Liquid-ordered phase formation in cholesterol-POPC bilayers: all-atom molecular dynamics simulations *Biophys. J.* **106** 80a

[50] Lindblom G, Orädd G and Filippov A 2006 Lipid lateral diffusion in bilayers with phosphatidylcholine, sphingomyelin and cholesterol—an NMR study of dynamics and lateral phase separation *Chem. Phys. Lipids* **141** 179–84
[51] Nichols-Smith S, The S-Y and Kuhl T 2004 Thermodynamic and mechanical properties of model mitochondrial membranes *Biochim. Biophys. Acta* **1663** 82–8
[52] Chen Q and Li Q 2001 Effect of cardiolipin on proton permeability of phospholipid liposomes: the role of hydration at the lipid-water interface *Arch. Biochem. Biophys.* **389** 201–6
[53] Tari A and Huang L 1989 Structure and function relationship of phosphatidylglycerol in the stabilization of the phosphatidylethanolamine bilayer *Biochemistry* **28** 7708–12
[54] Sparrman T and Westlund P 2003 An NMR line shape and relaxation analysis of heavy water powder spectra of the L-alpha,
L-beta and P-beta phases in the DPPC/water system *Phys. Chem. Chem. Phys.* **5** 2114–21
[55] Knowles T P J and Buehler M J 2011 Nanomechanics of functional and pathological amyloid materials *Nat. Nanotechnol.* **6** 469–79
[56] Solar M and Buehler M J 2012 Comparative analysis of nanomechanics of protein filaments under lateral loading *Nanoscale* **4** 1177–83
[57] Biancalana M and Koide S 2010 Molecular mechanism of thioflavin-T binding to amyloid fibrils *Biochim. Biophys. Acta* **1804** 1405–12
[58] Groenning M, Olsen L, van de Weert M, Flink J M, Frokjaer S and Jorgensen F S 2007 Study on the binding of thioflavin T to beta-sheet-rich and non-beta-sheet cavities *J. Struct. Biol.* **158** 358–69
[59] Krebs M R, Bromley E H and Donald A M 2005 The binding of thioflavin-T to amyloid fibrils: localisation and implications *J. Struct. Biol.* **149** 30–7
[60] Demchenko A P 1982 On the nanosecond mobility in proteins: edge excitation fluorescence red shift of protein-bound 2-(p-toluidinylnaphthalene)-6-sulfonate *Biophys. Chem.* **15** 101–9
[61] Nelson R, Sawaya M R, Balbirnie M, Madsen A, Riekel C, Grothe R and Eisenberg D 2005 Structure of the cross-beta spine of amyloid-like fibrils *Nature* **435** 773–8
[62] Reddy G, Straub J E and Thirumalai D 2010 Dry amyloid fibril assembly in a yeast prion peptide is mediated by long-lived structures containing water wires *Proc. Natl Acad. Sci. USA* **107** 21459–64
[63] Haldar S, Raghuraman H and Chattopadhyay A 2008 Monitoring orientation and dynamics of membrane-bound melittin utilizing dansyl fluorescence *J. Phys. Chem.* B **112** 14075–82
[64] Kee H L *et al* 2005 Structural control of the photodynamics of boron-dipyrrin complexes *J. Phys. Chem.* B **109** 20433–43
[65] Shaffer R E 2002 Multi- and megavariate data analysis. Principles and applications *J. Chemometr.* **16** 261–2
[66] Inshyn D I, Kovalska V B, Losytskyy M Y, Slominskii Y I, Tolmachev O I and Yarmoluk S 2014 Development of a quantitative structure activity relations (QSAR) model to guide the design of fluorescent dyes for detecting amyloid fibrils *Biotech. Histochem.* **89** 1–7
[67] Cisek K and Kuret J 2012 QSAR studies for prediction of cross-β sheet aggregate binding affinity and selectivity *Bioorg. Med. Chem.* **20** 1434–41
[68] Wolfe L S *et al* 2010 Protein-induced photophysical changes to the amyloid indicator dye thioflavin T *Proc. Natl Acad. Sci.* **107** 16863–8